

pyisotopomer: A Python package for obtaining intramolecular isotope ratio differences from mass spectrometric analysis of nitrous oxide isotopocules

Colette Kelly¹, Cara Manning², Claudia Frey³, Jan Kaiser⁴, Noah Gluschankoff¹, and Karen Casciotti¹

¹Stanford University

²University of Connecticut

³University of Basel

⁴University of East Anglia

February 26, 2023

Abstract

RATIONALE Obtaining nitrous oxide isotopocule measurements with isotope ratio mass spectrometry (IRMS) involves analyzing the ion current ratios of the nitrous oxide parent ion (N_2O^+) as well as those of the NO^+ fragment ion. The data analysis requires correcting for “scrambling” in the ion source, whereby the NO^+ fragment ion obtains the outer N atom from the N_2O^+ molecule. While descriptions exist for this correction, and interlaboratory intercalibration efforts have been made, there has yet to be published a package of code for implementing isotopomer calibrations. **METHODS** We developed a user-friendly Python package (pyisotopomer) to determine two coefficients (γ and κ) that describe scrambling in the IRMS ion source, and then to use this calibration to obtain intramolecular isotope deltas in N_2O samples. **RESULTS** We show that, with two reference materials distinct enough in their site preference, γ and κ can be determined robustly and accurately for a given IRMS. An additional third reference material is needed to define the zero-point of the delta scale. We show that the scrambling behavior of an IRMS can vary with time, necessitating regular calibrations. Finally, we present an intercalibration between two IRMS laboratories, using pyisotopomer to calculate γ and κ and to obtain intramolecular N_2O isotope deltas in lake water unknowns. **CONCLUSIONS** Given these considerations, we discuss how to use pyisotopomer to obtain high-quality N_2O isotopocule data from IRMS systems, including the use of appropriate reference materials and frequency of calibration.

In preparation for Rapid Communications in Mass Spectrometry
**pyisotopomer: A Python package for obtaining intramolecular isotope ratio differences
from mass spectrometric analysis of nitrous oxide isotopocules**

Colette L. Kelly,^{1*} Cara Manning,² Claudia Frey,³ Jan Kaiser,⁴ Noah Gluschankoff,¹ and Karen L. Casciotti

1. Stanford University, Department of Earth System Science, Stanford, CA 94305, USA

2. University of Connecticut, Department of Marine Sciences, Groton, CT, 06340, USA

3. Department of Environmental Science, University of Basel, Basel, Switzerland.

4. University of East Anglia, Centre for Ocean and Atmospheric Sciences, School of Environmental Sciences, Norwich, NR4 7TJ, UK

* **Correspondence to:** Colette L. Kelly (email: clkelly@stanford.edu; phone: 802-595-3647; address: 473 Via Ortega Room 140, Stanford, CA 94305).

Keywords: Nitrous oxide, isotopomers, isotopocules, scrambling, Python

Abstract

RATIONALE Obtaining nitrous oxide isotopocule measurements with isotope ratio mass spectrometry (IRMS) involves analyzing the ion current ratios of the nitrous oxide parent ion (N_2O^+) as well as those of the NO^+ fragment ion. The data analysis requires correcting for “scrambling” in the ion source, whereby the NO^+ fragment ion obtains the outer N atom from the N_2O molecule. While descriptions exist for this correction, and interlaboratory intercalibration efforts have been made, there has yet to be published a package of code for implementing isotopomer calibrations.

METHODS We developed a user-friendly Python package (pyisotopomer) to determine two coefficients (γ and κ) that describe scrambling in the IRMS ion source, and then to use this calibration to obtain intramolecular isotope deltas in N_2O samples.

RESULTS We show that, with two reference materials distinct enough in their site preference, γ and κ can be determined robustly and accurately for a given IRMS. An additional third reference material is needed to define the zero-point of the delta scale. We show that the scrambling behavior of an IRMS can vary with time, necessitating regular calibrations. Finally, we present an intercalibration between two IRMS laboratories, using pyisotopomer to calculate γ and κ , and to obtain intramolecular N_2O isotope deltas in lake water unknowns.

CONCLUSIONS Given these considerations, we discuss how to use pyisotopomer to obtain high-quality N_2O isotopocule data from IRMS systems, including the use of appropriate reference materials and frequency of calibration.

1. Introduction

Nitrous oxide (N₂O) is a potent greenhouse gas, with a global warming potential 265 times that of carbon dioxide over a 100 year time horizon^{1,2}. N₂O is also likely to be the most emitted ozone depletion agent in the 21st century, due to production of NO radicals in the stratosphere that interact destructively with ozone^{3–6}. Historically, the bulk stable isotopes of nitrogen and oxygen in N₂O have been used to quantify its microbial cycling in soils^{7,8} and in the ocean^{9–12}, its destruction by photolysis and O(¹D), and its cycling in the atmosphere^{13,14}. This approach often fails to provide a unique solution, because the bulk nitrogen and oxygen isotope ratios of N₂O depend on the isotopic composition of the substrate, as well as the isotope effects of production and consumption processes¹². Furthermore, in the context of microbial N₂O cycling in soils and the ocean, bacterial nitrification and denitrification produce N₂O with similar bulk $\delta(^{15}\text{N})^1$ values, preventing partitioning between these processes on the basis of bulk $\delta(^{15}\text{N})$ alone^{15,16}.

The site-specific nitrogen isotope ratios of N₂O provide a more nuanced constraint on the biogeochemical cycling of N₂O than its bulk composition alone. N₂O isotopomers have been used extensively to quantify its biogeochemical cycling in soils^{17–20}, the atmosphere^{14,21–23}, and the ocean^{24–34}. The individual isotopic compositions of each nitrogen atom were first measured by Friedman and Bigeleisen, who quantified the yields of isotopomers ¹⁴N¹⁵N¹⁶O and ¹⁵N¹⁴N¹⁶O from enriched ammonium nitrate by measuring the NO⁺ fragment ion signal in an isotope ratio mass spectrometer (IRMS)³⁵. 50 years later, these N₂O isotopomers were quantified at natural abundance from the N₂O⁺ species with mass numbers 44, 45, and 46 and the mass 30 and 31 NO⁺ fragment ion^{36,37}. The central nitrogen atom in the N₂O molecule has been designated with locants α , μ , or 2; the terminal atom, with locants β , τ , or 1^{38,39}. Here, we use the definitions from Toyoda and Yoshida (1999) for the site-specific isotope number (N) ratios of the central (α) nitrogen atom and terminal (β) nitrogen atom³⁶:

$$^{15}R^{\alpha} = \frac{N(^{14}\text{N}^{15}\text{NO})}{N(^{14}\text{N}^{14}\text{NO})} \quad (1)$$

$$^{15}R^{\beta} = \frac{N(^{15}\text{N}^{14}\text{NO})}{N(^{14}\text{N}^{14}\text{NO})} \quad (2)$$

The N₂O isotopomer measurement was initially performed with two sequential measurements of the same sample on an isotope ratio mass spectrometer, one at m/z 44, 45, and 46, and the other at m/z 30 and 31³⁶. Use of dedicated cup-configurations on lower-dispersion IRMS instruments allowed simultaneous analysis of all five masses together⁴⁰.

The slight difference in absorption cross sections between the isotopocules of N₂O result in different isotopic fractionations during photolysis and photo-oxidation in the stratosphere⁴¹, making the isotopomers of N₂O a powerful tool for understanding its atmospheric cycling^{21,42–45}. Likewise, N₂O site preference, defined as $\delta(^{15}\text{N}^{\text{sp}}) = \delta(^{15}\text{N}^{\alpha}) - \delta(^{15}\text{N}^{\beta})$, was shown in microbial culture experiments to be largely a function of reaction mechanism, independent of source composition^{24,46–50}. This allowed for the differentiation between N₂O from bacterial nitrification and denitrification, although some debate exists about whether the site preference of N₂O produced by denitrifying bacteria is closer to 0 ‰ or 25 ‰^{49,51}, the latter possibility being largely

¹ We write δ values with parentheses, e.g., $\delta(^{15}\text{N})$, because δ is the quantity symbol and “¹⁵N” is the label. See SI Brochure: <https://www.bipm.org/en/publications/si-brochure/>

ignored in subsequent literature. During N₂O consumption, $\delta(^{15}\text{N}^\alpha)$ and $\delta(^{18}\text{O})$ were shown in microbial culture⁵² and soil mesocosm¹⁹ experiments to exhibit a characteristic relationship, allowing subsequent studies to use this relationship to distinguish between oxidative and reductive regimes of N₂O cycling^{30,33}.

Site-specific nitrogen isotope ratio measurements based on mass spectrometry need to be corrected for a phenomenon called “scrambling,” whereby the NO⁺ fragment ion contains the terminal N atom, rather than the central N attached to the O atom (as in the original molecule). A number of approaches have been taken to calibrate an IRMS system for this effect: the use of a single “rearrangement factor” to describe scrambling^{36,53}, the use of nine coefficients to describe the different fragmentation behaviors of the different isotopocules of N₂O⁵⁴, and finally the use of two coefficients to describe scrambling in the ion source⁵⁰. While descriptions exist for each of these approaches, and interlaboratory intercalibration efforts have been made^{55,56}, there has yet to be published a package of code for implementing one of the above isotopomer calibrations.

We developed a Python software package that implements the two-coefficient approach described by Frame and Casciotti³² to calibrate an IRMS for scrambling and use that calibration to obtain high-quality N₂O isotopocule data. This software solves a set of equations, either analytically or with an optimization routine, to quantify the scrambling behavior of an IRMS. To quantify the performance of the software, we tested the sensitivity of the analytical and optimization-based solutions to their input conditions and assessed when each method is most appropriate. To quantify the variability of the fragmentation behavior of an instrument over time, we examined the scrambling behavior of one IRMS over the course of four years of measurements. We derived a simplified equation and used a Monte Carlo simulation approach to quantify the effect of uncertainty in the scrambling coefficients on the final isotope deltas. Finally, we performed an intercalibration using this software across two labs, at Stanford University (‘Lab 1’) and the University of Basel (‘Lab 2’).

2. Mathematical framework

The molecular ion number ratios 45/44 (⁴⁵*R*) and 46/44 (⁴⁶*R*) can be written in terms of atomic isotope ratios as^{36,53}:

$$^{45}R = ^{15}R^\alpha + ^{15}R^\beta + ^{17}R \quad (3)$$

$$^{46}R = (^{15}R^\alpha + ^{15}R^\beta)^{17}R + ^{18}R + ^{15}R^\alpha ^{15}R^\beta \quad (4)$$

where ¹⁵*R*^α, ¹⁵*R*^β, ¹⁷*R* and ¹⁸*R* denote the number ratios of ¹⁴N¹⁵N¹⁶O, ¹⁵N¹⁴N¹⁶O, ¹⁴N₂¹⁷O, and ¹⁴N₂¹⁸O, respectively, to ¹⁴N₂¹⁶O, assuming a stochastic isotope distribution between mono- and poly-substituted isotopocules.

For many N₂O samples, ¹⁷*R* covaries with ¹⁸*R* according to the oxygen isotope ratios of Vienna Standard Mean Ocean Water (VSMOW)^{57,58} and a mass-dependent relationship between ¹⁷*R* and ¹⁸*R* with coefficient $\beta = 0.516$ ⁵⁹. Deviations from this relationship are expressed by the oxygen triple isotope excess $\Delta(^{17}\text{O})$ ^{59–61}, which provides additional information about the sources and sinks of N₂O^{59,62}:

$$^{17}R / ^{17}R_{\text{VSMOW}} = (^{18}R / 0.0020052)^\beta [\Delta(^{17}\text{O}) + 1] \quad (5)$$

The simplest formulation for the NO⁺ fragment ion number ratio 31/30 (³¹*R*) is given as³⁶:

$$^{31}R = ^{15}R^\alpha + ^{17}R \quad (6)$$

This equation would represent the ^{31}R measured by IRMS if no scrambling occurred. To describe instead the scrambled ^{31}R , Toyoda and Yoshida³⁶ define the rearrangement factor γ (which was later given the symbol γ) as “the fraction of NO^+ bearing the β nitrogen of the initial N_2O to the total NO^+ formed,” to yield:

$$^{31}R = (1 - \gamma)^{15}R^\alpha + \gamma^{15}R^\beta + ^{17}R \quad (7)$$

where $^{15}R^\alpha$ and $^{15}R^\beta$ represent atomic isotope ratios of the sample. In other words, γ relates the scrambled NO^+ fragment ratio to the unscrambled $^{15}R^\alpha$ and $^{15}R^\beta$ of the sample.

Kaiser et al.⁵³ introduced a more complete representation of ^{31}R , adding terms for $^{15}\text{N}^{15}\text{N}^{16}\text{O}$, $^{14}\text{N}^{15}\text{N}^{17}\text{O}$, and $^{15}\text{N}^{14}\text{N}^{17}\text{O}$ to m/z 31, and terms for $^{15}\text{N}^{14}\text{N}^{16}\text{O}$ and $^{14}\text{N}^{15}\text{N}^{16}\text{O}$ to m/z 30:

$$\begin{aligned} ^{31}R &= (1 - \gamma)^{15}R^\alpha + \gamma^{15}R^\beta + ^{17}R - \frac{\gamma(1 - \gamma)(^{15}R^\alpha - ^{15}R^\beta)^2}{1 + \gamma^{15}R^\alpha + (1 - \gamma)^{15}R^\beta} \\ &= \frac{(1 - \gamma)^{15}R^\alpha + \gamma^{15}R^\beta + ^{15}R^\alpha^{15}R^\beta + ^{17}R[1 + \gamma^{15}R^\alpha + (1 - \gamma)^{15}R^\beta]}{1 + \gamma^{15}R^\alpha + (1 - \gamma)^{15}R^\beta} \end{aligned} \quad (8)$$

Note that Kaiser et al.⁵³ use the symbol “ s ” for γ , $^{15}R_1$ for $^{15}R^\beta$, and $^{15}R_2$ for $^{15}R^\alpha$.

To account for different fragmentation rates of different N_2O isotopocules, Westley et al.⁵⁴ replaced the rearrangement factor γ with nine separate coefficients:

$$^{31}R = \frac{a_{31}^{15}R^\alpha + b_{31}^{15}R^\beta + c_{31}^{15}R^\alpha^{15}R^\beta + ^{17}R[d_{31} + e_{31}^{15}R^\alpha + f_{31}^{15}R^\beta]}{1 + a_{30}^{15}R^\alpha + b_{30}^{15}R^\beta + c_{30}^{15}R^\alpha^{15}R^\beta} \quad (9)$$

While this approach considers the possibility of different rearrangement factors for every N_2O isotopocule as well as $^{15}\text{N}_2^+$ formation, it also requires solving for three to nine coefficients, depending on whether a_{30} , b_{30} and c_{30} , as well as d_{31} , e_{31} and f_{31} , are considered separately from coefficients a_{31} , b_{31} and c_{31} .

Frame and Casciotti⁵⁰ simplify this equation by reducing the number of rearrangement factors to two coefficients, γ and κ , which represent the yield of $^{14}\text{NO}^+$ from $^{14}\text{N}^{15}\text{N}^{16}\text{O}$ and $^{14}\text{N}^{15}\text{N}^{17}\text{O}$, and the yield of $^{15}\text{NO}^+$ from $^{15}\text{N}^{14}\text{N}^{16}\text{O}$, respectively. This produces the equation:

$$^{31}R = \frac{(1 - \gamma)^{15}R^\alpha + \kappa^{15}R^\beta + ^{15}R^\alpha^{15}R^\beta + ^{17}R[1 + \gamma^{15}R^\alpha + (1 - \kappa)^{15}R^\beta]}{1 + \gamma^{15}R^\alpha + (1 - \kappa)^{15}R^\beta} \quad (10)$$

The important pieces of information contained within the two scrambling factors are the unequal rates of fragmentation for the isotopomers $^{14}\text{N}^{15}\text{NO}$ and $^{15}\text{N}^{14}\text{NO}$, which eqns. (7) and (8) assume are equal. Eqn. (10) is formulated by assuming that the ^{17}O -isotopocules have the same scrambling behavior as the ^{16}O -isotopocules, i.e., $e_{31} = 1 - a_{31}$ and $f_{31} = 1 - b_{31}$, in terms of the coefficients in eqn. (9). It is also assumed that $c_{31} = 1$, i.e., the yield of $^{15}\text{N}^{16}\text{O}^+$ from $^{15}\text{N}_2^{16}\text{O}$ is equal to the yield of $^{14}\text{N}^{16}\text{O}^+$ from $^{14}\text{N}_2^{16}\text{O}$. Given that naturally occurring N_2O contains very little $^{15}\text{N}_2^{16}\text{O}$, a small difference in this yield would not significantly alter ^{31}R .⁶³ Finally, it is assumed that $d_{31} = 1$, or that the yield of $^{14}\text{N}^{17}\text{O}^+$ from $^{14}\text{N}_2^{17}\text{O}$ is equal to the yield of $^{14}\text{N}^{16}\text{O}^+$ from $^{14}\text{N}_2^{16}\text{O}$; again, an assumption yielding little error in ^{31}R , given the low natural abundance of ^{17}O in N_2O .⁵⁹

Eqn. (10) can be rearranged to give an equation for γ as a function of κ (the full derivation is presented in Supplementary text S1):

$$\gamma = \frac{^{15}R^\alpha + \kappa^{15}R^\beta + ^{15}R^\alpha^{15}R^\beta - (^{31}R - ^{17}R)[1 + (1 - \kappa)^{15}R^\beta]}{^{15}R^\alpha(1 + (^{31}R - ^{17}R))} \quad (11)$$

151 For two reference materials, we can write two such equations and solve for two
 152 unknowns, γ and κ . $^{15}R^\alpha$ and $^{15}R^\beta$ represent *known* values for each reference material, and ^{31}R is
 153 the observed quantity. Essentially, we are asking what values of γ and κ for a pair of known $^{15}R^\alpha$
 154 and $^{15}R^\beta$ values gives the observed ^{31}R for each reference gas. Setting the two solutions for γ
 155 equal allows us to determine κ and γ algebraically from the assigned ^{15}R values of reference
 156 materials 1 and 2 ($^{15}R_1^\alpha$, $^{15}R_1^\beta$, $^{15}R_2^\alpha$, $^{15}R_2^\beta$), their observed ^{31}R values ($^{31}R_1$, $^{31}R_2$), and the ^{17}R
 157 values ($^{17}R_1$, $^{17}R_2$):

$$\kappa = \frac{\frac{(^{15}R_1^\alpha - ^{31}R_1 + ^{17}R_1)(1 + ^{15}R_1^\beta)}{^{15}R_1^\alpha(1 + ^{31}R_1 - ^{17}R_1)} - \frac{(^{15}R_2^\alpha - ^{31}R_2 + ^{17}R_2)(1 + ^{15}R_2^\beta)}{^{15}R_2^\alpha(1 + ^{31}R_2 - ^{17}R_2)}}{\frac{^{15}R_2^\beta}{^{15}R_2^\alpha} - \frac{^{15}R_1^\beta}{^{15}R_1^\alpha}} \quad (12a)$$

$$\gamma = \frac{\frac{(^{15}R_1^\alpha - ^{31}R_1 + ^{17}R_1)(1 + ^{15}R_1^\beta)}{^{15}R_1^\alpha(1 + ^{31}R_1 - ^{17}R_1)} \left(\frac{^{15}R_2^\beta}{^{15}R_2^\alpha} \right) - \frac{(^{15}R_2^\alpha - ^{31}R_2 + ^{17}R_2)(1 + ^{15}R_2^\beta)}{^{15}R_2^\alpha(1 + ^{31}R_2 - ^{17}R_2)} \left(\frac{^{15}R_1^\beta}{^{15}R_1^\alpha} \right)}{\frac{^{15}R_2^\beta}{^{15}R_2^\alpha} - \frac{^{15}R_1^\beta}{^{15}R_1^\alpha}} \quad (12b)$$

158 After substituting $^{45}R - ^{15}R^\alpha - ^{15}R^\beta$ for ^{17}R , the equations for γ and κ can also be written as
 159 follows:

$$\kappa = \frac{\frac{(^{45}R_1 - ^{31}R_1 - ^{15}R_1^\beta)(1 + ^{15}R_1^\beta)}{^{15}R_1^\alpha(1 + ^{15}R_1^\alpha + ^{15}R_1^\beta + ^{31}R_1 - ^{45}R_1)} - \frac{(^{45}R_2 - ^{31}R_2 - ^{15}R_2^\beta)(1 + ^{15}R_2^\beta)}{^{15}R_2^\alpha(1 + ^{15}R_2^\alpha + ^{15}R_2^\beta + ^{31}R_2 - ^{45}R_2)}}{\frac{^{15}R_2^\beta}{^{15}R_2^\alpha} - \frac{^{15}R_1^\beta}{^{15}R_1^\alpha}} \quad (13a)$$

$$\gamma = \frac{\frac{(^{45}R_1 - ^{31}R_1 - ^{15}R_1^\beta)(1 + ^{15}R_1^\beta)}{^{15}R_1^\alpha(1 + ^{15}R_1^\alpha + ^{15}R_1^\beta + ^{31}R_1 - ^{45}R_1)} \left(\frac{^{15}R_2^\beta}{^{15}R_2^\alpha} \right) - \frac{(^{45}R_2 - ^{31}R_2 - ^{15}R_2^\beta)(1 + ^{15}R_2^\beta)}{^{15}R_2^\alpha(1 + ^{15}R_2^\alpha + ^{15}R_2^\beta + ^{31}R_2 - ^{45}R_2)} \left(\frac{^{15}R_1^\beta}{^{15}R_1^\alpha} \right)}{\frac{^{15}R_2^\beta}{^{15}R_2^\alpha} - \frac{^{15}R_1^\beta}{^{15}R_1^\alpha}} \quad (13b)$$

161 To obtain $^{31}R_1$ and $^{31}R_2$ in continuous-flow analysis, we measure two reference materials
 162 against a common working reference gas (wr), which is calibrated independently. The working
 163 reference is a third calibrated reference material that normalizes different runs to the same
 164 reference frame:

$$^{31}R_1 = (1 + ^{31}\delta_1)^{31}R_{wr} \quad (14)$$

$$^{31}R_2 = (1 + ^{31}\delta_2)^{31}R_{wr} \quad (15)$$

166 where $^{31}R_1$ and $^{31}R_2$ are calculated values that depend on γ and κ ; $^{31}\delta$ is the measured ion
 167 current ratio difference of sample (1 or 2) to working reference peak, and $^{31}R_{wr}$ is an assumed

value calculated with constant γ and κ and assigned $^{15}R^\alpha$, $^{15}R^\beta$, and ^{17}R . Calculating $^{31}R_{wr}$ with constant γ and κ assumes that the working reference peak experiences a defined scrambling behavior that could differ from that of a sample peak; ultimately, however, $^{31}R_{wr}$ drops out of the final $\delta(^{15}\text{N}^{sp})$ calculation, so this assumption has little effect.

The “algebraic” solution in pyisotopomer⁶⁴ uses $^{31}R_1$ and $^{31}R_2$ in eqns. (11) and (12) to obtain γ and κ . The “least_squares” method in pyisotopomer⁶⁴ solves eqns. (14) and (15) for γ and κ iteratively with a least squares optimization routine. We present a full discussion of the appropriate use of the algebraic and least squares methods in section 4.2.

Some of the isotopomer literature obtains $^{15}R^{bulk}$ and $^{15}R^\alpha$ by regression between true and measured values of reference materials, inferring $^{15}R^\beta$ indirectly²⁰. In this case, a linear calibration curve replaces the scrambling correction. A linear calibration curve is only acceptable if the unknowns are close in their $\delta(^{15}\text{N}^{sp})$ to those of the reference material — although in this case, it may not even be necessary to use a more than one reference material. It is not accurate if unknowns diverge in their $\delta(^{15}\text{N}^{sp})$ from that of the reference material(s). This is because the measured $^{31}\delta$ value depends on both $^{15}R^\alpha$ and $^{15}R^\beta$ (Supplementary text S2).

To obtain $^{15}R^\alpha$, $^{15}R^\beta$, and ^{18}R of unknowns, pyisotopomer solves for these values from eqns. (3), (4), (5), and (10), using ^{31}R , ^{45}R , ^{46}R , γ , and κ as input terms⁵⁰. The delta values $\delta(^{15}\text{N}^\alpha)$, $\delta(^{15}\text{N}^\beta)$, $\delta(^{15}\text{N}^{sp})$, $\delta(^{15}\text{N}^{bulk})$, and $\delta(^{18}\text{O})$ are calculated from $^{15}R^\alpha$, $^{15}R^\beta$, and ^{18}R relative to primary reference scales (^{15}R from atmospheric N_2 and ^{18}R from VSMOW; if desired, the values of primary reference scale ratios may be adjusted with keyword arguments, as described in the pyisotopomer Documentation⁶⁴). Additionally, if $\Delta^{17}\text{O}$ has been measured separately^{59,61,62}, pyisotopomer can take this value into account in the calculation of $\delta(^{15}\text{N}^\alpha)$, $\delta(^{15}\text{N}^\beta)$, $\delta(^{15}\text{N}^{sp})$, $\delta(^{15}\text{N}^{bulk})$, and $\delta(^{18}\text{O})$.

3. Experimental methods

3.1 Preparation and analysis of dissolved N_2O reference materials

A series of dissolved N_2O reference materials (Table 1) were prepared and analyzed in both Lab 1 and Lab 2. Reference materials were prepared by filling 160-mL glass serum bottles (Wheaton) with de-ionized water and removing a 4-mL headspace (Lab 1) or 10 to 20-mL headspace (Lab 2), then capped with a gray butyl rubber septum (National Scientific) and sealed with an aluminum crimp seal. These bottles were purged with helium for 90 minutes at yields a minimum flow rate of 100 mL/min to remove all background N_2O . The purged bottles were then injected with 2 to 43 nmol N_2O (Lab 1) or 1 to 60 nmol N_2O (Lab 2) in a matrix of He or synthetic air (Table 1) using a gas-tight syringe. Reference materials prepared in Lab 1 were preserved with 100 μL saturated mercuric chloride (HgCl_2) solution; those prepared in Lab 2 contained no added preservative. For Lab 1, atmosphere-equilibrated seawater was prepared by filtering surface seawater (collected in Half Moon Bay, CA) through a 0.22 mm Sterivex filter, allowing it to undergo static equilibration with outdoor air for three days, then re-filtering into 160-mL serum bottles, removing a 1-mL headspace, and preserving with 100 μL saturated mercuric chloride solution. For Lab 2, atmosphere-equilibrated reference materials were prepared by purging either de-ionized water or a sodium chloride solution with helium, allowing it to undergo static equilibration with outdoor air for three days, filling into 160-mL serum bottles, and removing a 10-mL headspace. Reference materials were run in the same format as samples to account for any potential fractionation associated with the purge-and-trap system. The magnitude of such fractionation was quantified for Lab 1 by running aliquots of the pure N_2O reference tank in sample format; this test yielded offsets of $(0.22 \pm 0.52) \text{‰}$ for $\delta(^{15}\text{N}^{bulk})$ and

(0.16±0.62) ‰ for $\delta(^{18}\text{O})$ vs. the reference tank injection (see Supplementary text S3 for a full discussion of potential fractionation effects in the purge-and-trap system).

The reference gases were calibrated independently by J. Mohn (EMPA; mini-QCLAS aerodyne) or S. Toyoda (Tokyo Tech; IRMS), except for one internal standard used by Lab 1 (B6; Table 1). The $\delta(^{17}\text{O})$ values for each gas were calculated assuming a mass-dependent relationship between ^{17}R and ^{18}R (eqn. 5).

Reference gases and samples were measured on Thermo Finnigan DELTA V Plus isotope ratio mass spectrometers (IRMS; Thermo Fisher Scientific, Waltham, MA) in Labs 1 and 2. Each IRMS had Faraday cups configured to simultaneously measure m/z 30, 31, 44, 45, and 46. Reference materials and samples were analyzed on custom purge-and-trap systems coupled to each IRMS, which was run in continuous flow mode⁶⁵ (Table 1). The two systems had slight differences in the purge-and-trap method: in Lab 1, liquid from each sample bottle was transferred under helium pressure to a sparging column to extract the dissolved gases⁶⁶; in Lab 2, each sample was extracted by purging directly from the bottle. The effects of these differences are discussed further in Results and Discussion.

3.2 Data corrections

3.2.1 Linearity relation

The measured ion current ratios 31/30, 45/44, and 46/44 of each sample peak were divided by those of the working reference peak. This produced three molecular isotope delta values $^{31}\delta+1$, $^{45}\delta+1$, and $^{46}\delta+1$, where $\delta = R_s/R_{wr} - 1$, with the subscripts “s” and “wr” denoting sample and working reference, respectively (Figure 1, Step 5).

The δ values were corrected for the effect of peak size³³. For Lab 1, this was accomplished by running six reference materials (reference gases S2, B6, A01, CA06261, 90454, and 94321; Table 1) in size series ranging from 2-43 nmol N₂O. For Lab 2, three reference materials (CA06261, 53504, and CA08214) were run in size series ranging from 1-60 nmol N₂O (Figure 1, Step 6).

To obtain a single size correction slope from multiple size series, we used the dummy-variable method of combining regressions⁶⁷. The dummy variable method is an improvement over simply averaging each individually calculated slope because it implicitly weighs each size series by its informativeness, producing a slope that is more likely to reflect the overall linearity behavior of the instrument⁶⁷. For a given material, each measured $\delta+1$ is a linear function of its peak area (A) plus an intercept ($\gamma_1 + \gamma_2 D_2 + \gamma_3 D_3$):

$$\delta + 1 = \hat{\beta}A + \gamma_1 + \gamma_2 D_2 + \gamma_3 D_3 \quad (16)$$

where $\hat{\beta}$ represents the regression coefficient for a particular peak area (for m/z 31, 45, or 46), obtained by multiple linear regression. The intercept for reference material 1 is γ_1 . D_2 and D_3 are ‘dummy variables’ to adjust γ_1 by an appropriate intercept for reference material 2 ($\gamma_1 + \gamma_2$) and reference material 3 ($\gamma_1 + \gamma_3$). Thus, for reference material 1, $D_2 = D_3 = 0$; for reference material 2, $D_2 = 1$ and $D_3 = 0$; for reference material 3, $D_2 = 0$ and $D_3 = 1$. These dummy variables allow us to obtain one slope for each isotope delta from multiple datasets accounting for differences in intercept, with each reference material weighted by its spread in the x -axis range. Thus, slopes $\hat{\beta}_{31}$, $\hat{\beta}_{45}$, and $\hat{\beta}_{46}$ were calculated for $^{31}\delta+1$, $^{45}\delta+1$, and $^{46}\delta+1$, respectively, each using eqn. (16).

To normalize measured values of $\delta+1$ to a common peak area, we first calculated the $(\delta+1)_0$ that would be measured at m/z 44 peak area A_0 :

$$(\delta + 1)_0 = \hat{\beta}(A_0) + \gamma_1 + \gamma_2 D_2 + \gamma_3 D_3 \quad (17)$$

Note that $(\delta+1)_0$ is still a function of $\hat{\beta}$, the intercepts $\gamma_1, \gamma_2, \gamma_3$, and the dummy variables D_2 and D_3 . To obtain the difference $\delta_0 - \delta$ from the measured m/z 44 peak area A , we subtract eqn. (17) from eqn. (16), to obtain:

$$(\delta + 1)_0 - (\delta + 1) = \hat{\beta}(A_0 - A)$$

In this case, the size-corrected molecular isotope ratio, δ_0 , for each sample with measured δ and peak area A is given by:

$$(\delta + 1)_0 = \hat{\beta}(A_0 - A) + (\delta + 1) \quad (18)$$

Eqn. (18) is simply a function of the slope $\hat{\beta}$, the measured (A) and target (A_0) m/z 44 peak areas, and the measured δ . Thus, eqn. (18) can be applied across a range of peak areas and δ values to normalize these δ values to a common peak area. Using this method, we normalized the measured $^{31}\delta+1$, $^{45}\delta+1$, and $^{46}\delta+1$ of each sample to a peak area (A_0) of 20 Vs (Figure 1, Step 7).

3.2.2 Scale normalization and calculation of ^{17}R

After applying the linearity correction, a scale normalization was applied to $^{45}\delta$ and $^{46}\delta$ (Figure 1, Step 8). The scale normalization for $^{45}\delta$ and $^{46}\delta$ needs to be carried out before the scrambling correction (which is essentially a scale normalization of $^{31}\delta$); otherwise, the wrong bulk $^{15}\text{N}/^{14}\text{N}$ and $^{18}\text{O}/^{16}\text{O}$ ratios are implied. Furthermore, while the γ and κ calculations constrain the differences between $\delta(^{15}\text{N}^\alpha)$ and $\delta(^{15}\text{N}^\beta)$, their absolute values are governed by $\delta(^{15}\text{N}^{\text{bulk}})$, necessitating that the “correct”, normalized value of $^{45}\delta$ be input to the scrambling equations. This scale normalization is a replacement for any scale normalization or offset correction to the final output δ values, such as the one-point and two-point offset corrections calculated and applied in Mohn et al. (2014).

A scale normalization was calculated for each run included in the intercalibration exercise. Since assigned values of ^{45}R and ^{46}R for each reference gas were unavailable, assigned ^{45}R and ^{46}R were calculated from assigned $^{15}R^\alpha$, $^{15}R^\beta$, and ^{18}R and eqns. (3), (4), and (5) (Table 1), assuming $^{17}R_{\text{VSMOW}} = 0.0003799^{68}$ and $^{18}R_{\text{VSMOW}} = 0.0020052^{57}$. Next, the assigned ^{45}R and ^{46}R for each reference gas were divided by the known ^{45}R and ^{46}R of the direct N_2O reference injection to obtain assigned $^{45}\delta$ and $^{46}\delta$ for each reference material. Then, these assigned $^{45}\delta$ and $^{46}\delta$ values were compared to measured $^{45}\delta$ and $^{46}\delta$ values, and scale normalization coefficients were calculated following the logarithmic scale normalization outlined in Kaiser et al. (2007):

$$\ln(1 + ^{45}\delta^n) = m \ln(1 + ^{45}\delta) + b$$

where $^{45}\delta^n$ is the normalized $^{45}\delta$, “ m ” is the slope of the regression of $\ln(1 + ^{45}\delta^n)$ vs. $\ln(1 + ^{45}\delta)$, and “ b ” is the intercept (and likewise for $^{46}\delta$). From this regression, the normalized δ values can be obtained:

$$1 + ^{45}\delta^n = e^b (1 + ^{45}\delta)^m \quad (19)$$

For the working reference, the values of $^{45}\delta$ and $^{45}\delta^n$ are equal to zero, so the intercept b should be equal to or very close to zero. The benefit of the logarithmic normalization is that, unlike a linear scale normalization, it is scale-invariant⁶¹: essentially, the logarithmic scale normalization does not skew the data towards extremely high or low values, and instead equally weights all data points⁶¹.

Next, a measured ^{18}R was derived from the scale-normalized ^{45}R and ^{46}R for each sample and reference material (Figure 1, Step 8). The size correction and scale normalization were carried out in the pyisotopomer spreadsheet template; the ^{18}R derivation from the scale-normalized ^{45}R and ^{46}R was the first step accomplished by the pyisotopomer code⁶⁴. Deriving ^{18}R

was accomplished by assuming a mass-dependent relationship between ^{17}R and ^{18}R (eqn. 5) and $^{15}R^{\alpha} = ^{15}R^{\beta} = ^{15}R^{\text{bulk}}$. These terms are then substituted into eqns. (3) and (4) to yield:

$$^{45}R = 2^{15}R^{\text{bulk}} + ^{17}R_{\text{VSMOW}} \left(\frac{^{18}R}{^{18}R_{\text{VSMOW}}} \right)^{\beta} (\Delta^{17}\text{O} + 1) \quad (20)$$

$$^{46}R = ^{18}R + 2^{15}R^{\text{bulk}} \left[^{17}R_{\text{VSMOW}} \left(\frac{^{18}R}{^{18}R_{\text{VSMOW}}} \right)^{\beta} (\Delta^{17}\text{O} + 1) \right] + (^{15}R^{\text{bulk}})^2 \quad (21)$$

Note that the slope β of the mass-dependent relationship between ^{17}R and ^{18}R is an adjustable parameter in the code (default: 0.516), and $\Delta^{17}\text{O}$ for each reference material may be entered in the data correction template and subsequently accounted for in this correction (default: 0 ‰). Eqns. (20) and (21) were then solved for ^{18}R and $^{15}R^{\text{bulk}}$ to obtain an estimated ^{18}R and $^{15}R^{\text{bulk}}$ for each sample and reference material, and ^{17}R was calculated from ^{18}R according to eqn. (5). The resulting ^{18}R , ^{17}R , and $^{15}R^{\text{bulk}}$ were used in the scrambling calculation. They contain an error due to the assumption that $^{15}R^{\alpha} = ^{15}R^{\beta} = ^{15}R^{\text{bulk}}$, although the magnitude of this error should be small⁶¹. Later, the isotopomer calculation solves for $^{15}R^{\alpha}$ and $^{15}R^{\beta}$ separately and thus corrects this error.

In the intercalibration exercise, values of m and b were calculated from the slopes of assigned $^{45}\delta^{\text{a}}$ vs. measured $^{45}\delta$ and assigned $^{46}\delta^{\text{a}}$ vs. measured $^{46}\delta$ from the reference materials in each run. These runs took place in February 2021 for Lab 1 and August 2020 and November 2020 for Lab 2. Combined, the scale normalization and size correction should account for any size- or isotope-ratio dependent effects, including those of a blank, linearity, or fractionation in the GasBench.

3.2.3 Calculating $^{31}R_{\text{m}}$ of the direct N_2O reference injection

We used the same scrambling coefficients for the working reference gas as for the samples. We recommend that the user calculates the ^{31}R of the direct reference injection ($^{31}R_{\text{wr}}$ in eqns. 14 and 15) with the following sequence of steps: 1) calculate $^{31}R_{\text{wr}}$ from eqn. (10) with either $\gamma = \kappa = 0.1$ or an *a priori* estimate, if available (Figure 1, Step 9); 2) use that $^{31}R_{\text{wr}}$ to correct data from two reference materials and from those reference materials, obtain γ and κ from eqns. (11) and (12) (Figure 1, Step 10); 3) use these updated γ and κ to re-calculate $^{31}R_{\text{wr}}$ from eqn. (10) (Figure 1, Step 11). The input γ and κ (used to calculate $^{31}R_{\text{wr}}$) and output γ and κ (calculated from paired reference materials) should converge quickly, so one iteration of this process should be sufficient. This value of $^{31}R_{\text{wr}}$ can then be used to convert $^{31}\delta$ to $^{31}R_{\text{s}}$. The user should also note that there are likely to be multiple pairings of input and output γ and κ that will consistently yield indistinguishable delta values.

3.2.4 IRMS scrambling calibration and isotopomer calculation

The "Scrambling" function of pyisotopomer was used to calculate γ and κ algebraically from all possible pairings of reference materials CA08214 and 53504 measured on a given IRMS (Lab 1 or Lab 2; Figure 1, Step 13). The reference materials CA08214 and 53504 were chosen because of their 113 ‰ $\delta(^{15}\text{N}^{\text{sp}})$ difference (see Results and Discussion for a description of how to choose reference material pairings), as well as the range of $\delta(^{15}\text{N}^{\alpha})$, $\delta(^{15}\text{N}^{\beta})$, $\delta(^{15}\text{N}^{\text{bulk}})$, and $\delta(^{18}\text{O})$ spanned by the two reference materials, which represent values found typically in culture^{52,69} and nature^{26,31}. One-week running averages of γ and κ were calculated to smooth their variation and used to obtain position-dependent δ values for unknowns and reference materials

run as unknowns for quality control (CA06261, S2, B6, and atmosphere-equilibrated seawater), using the "Isotopomers" function of pyisotopomer (Figure 1, Step 14).

For comparison, this exercise was repeated, calculating γ and κ iteratively with the least squares optimization (Figure 1, Step 12). The mean algebraic γ and κ from the paired reference materials CA08214 and 53504 was used as the initial guess for the least squares solver. In this case, reference materials CA08214 and CA06261 were used to calculate the least squares γ and κ , because these reference materials are close in their calibrated isotopomer values to natural abundance unknowns. As above, γ and κ were combined into a one-week running average; these running averages of γ and κ for each system were used to obtain position-dependent δ values for reference materials and unknowns in the intercalibration exercise (Figure 1, Step 14). The analytical precisions of $\delta(^{15}\text{N}^\alpha)$, $\delta(^{15}\text{N}^\beta)$, $\delta(^{15}\text{N}^{\text{sp}})$, $\delta(^{15}\text{N}^{\text{bulk}})$, and $\delta(^{18}\text{O})$ produced by each method are presented in the Results and Discussion.

N_2O amounts were obtained from the m/z 44 peak area and instrument N_2O sensitivity⁶⁶. To obtain the conversion factor between peak area and amount of N_2O , the peak areas for reference material amounts from 1 to 40 nmol N_2O were recorded. Standard deviations for inferred N_2O amounts of replicate unknown samples were 0.07 nmol for Lab 1, and 0.19 nmol for Lab 2. All data corrections are described in the README documents associated with pyisotopomer on the Python Package Index⁶⁴.

3.3 Lake water unknowns

To validate the scrambling calibration, samples of unknown isotopic composition were collected from Lake Lugano, Switzerland in July 2020 and analyzed separately by both Lab 1 and Lab 2. The samples were collected at depths of 10 and 90 meters, including six replicate bottles at each depth. Samples were collected into 160-mL glass serum bottles (Wheaton), overflowing each bottle twice, closing bubble-free, and removing liquid to form a 10-mL headspace comprised of air. Based on the northern hemisphere monthly mean tropospheric N_2O mole fraction when the samples were collected in July, 2020⁷⁰, an atmospheric headspace of this volume would have contained 0.13 nmol N_2O . For Lab 2, where the full amount of N_2O in the sample is measured, incorporation of the headspace into the measurement results in a 0.13 nmol overestimation of the amount of N_2O in the sample. For Lab 1, where 2 mL sample liquid is left behind post-analysis, equilibration the 10-mL headspace during sample storage results in either an underestimate (0.12 nmol) or overestimate (0.10 nmol) of N_2O in the sample, depending on its concentration. In both cases, these errors are similar to the analytical precision of the N_2O amount measurement. Each sample was capped with a gray butyl septum (National Scientific) and sealed with an aluminum crimp seal. Samples were promptly preserved with 100 μL saturated mercuric chloride solution and stored at lab temperature (20–22°C). The isotope effect associated with N_2O partitioning between the gas and liquid phases falls within the analytical uncertainty³³. The six replicate bottles at each depth were split into two groups of three replicate bottles to be measured by Lab 1 and Lab 2, respectively.

4. Results and Discussion

4.1 Linearity relation

Linearity relations were calculated using the dummy variable method described in Section 3.2.1 and applied to the intercalibration data as follows. A linearity relation was determined for Lab 1 in February 2021 (Figure 2a-c) and applied to lake water samples run in

Lab 1 and reference materials prepared and run in Lab 1. Reference materials prepared in Lab 2 but run in Lab 1 exhibited statistically distinct linearity slopes from those both prepared and run in Lab 1; thus, a separate linearity relation was applied to these reference materials (but not to the lake water samples) (Figure 2d-f). A linearity relation was determined for Lab 2 in May 2020 (Figure 2g-i) and applied to lake water samples and reference materials run in Lab 2. As previously observed⁷¹, for each linearity relation, the slopes of the fits for individual reference materials were identical within error. The linearity correction reduced the spread of measured molecular isotope ratios across size series of each given reference material (Figure S2).

4.2 IRMS scrambling calibration

For both labs, the “algebraic” solution produced reasonable values of γ and κ (i.e., between 0 and 1) for reference material pairings involving the reference material 53504 ($\delta(^{15}\text{N}^{\text{sp}}) = -93\text{‰}$). The mean γ and κ calculated for Lab 1 from reference materials 53504 and CA08214 were 0.174 ± 0.022 and 0.083 ± 0.022 , respectively (Table S2). In August 2020, the mean γ and κ calculated for Lab 2 from the same two reference materials were 0.095 ± 0.011 and 0.091 ± 0.010 , respectively; in November 2020, γ and κ for Lab 2 shifted to 0.091 ± 0.013 and 0.086 ± 0.013 , respectively (Table S2). Other reference materials paired with 53504 produced similar values of γ and κ . The difference $\gamma - \kappa$ was also consistent for reference material pairings with 53504: for Lab 1, $\gamma - \kappa$ was 0.090-0.091, and for Lab 2, it was 0.003-0.005 (Table S2).

For pairings with 53504, the $\delta(^{15}\text{N}^{\text{sp}})$ difference between both reference materials was greater than 100 ‰. Pairs of reference materials with smaller $\delta(^{15}\text{N}^{\text{sp}})$ differences produced more variable γ and κ values with the algebraic solution, which sometimes fell outside the physically plausible range between 0 and 1. For example, in Lab 1, the pairing of CA06261 and CA08214 produced γ and κ values of 0.01 ± 0.23 and -0.08 ± 0.23 , respectively. In this case, the measurement uncertainty was too large — and the $\delta(^{15}\text{N}^{\text{sp}})$ values too close — for the scrambling coefficients to be adequately determined. What matters, however, is that the difference between γ and κ is accurate; as the results show, the absolute values are less important (and can even be negative, greater than 1, or otherwise “unphysical”).

To understand the uncertainty in γ and κ calculated from equations 11 and 12, we define a variable d :

$$d = \frac{(^{15}\text{R}^{\beta} + ^{31}\text{R} - ^{45}\text{R})(1 + ^{15}\text{R}^{\beta})}{^{15}\text{R}_{\text{atm}}(1 + ^{15}\text{R}^{\alpha} + ^{15}\text{R}^{\beta} + ^{31}\text{R} - ^{45}\text{R})} \quad (22)$$

The value of d is similar for all samples and reference gases run on a given IRMS and depends primarily on the difference $^{31}\text{R} - ^{45}\text{R}$. Using δ notation, i.e., $\delta(^{15}\text{N}) = ^{15}\text{R}/^{15}\text{R}_{\text{atm}} - 1$, and dropping the label “ ^{15}N ” for brevity, eqns. (13a) and (13b) can be written as follows:

$$\kappa = \frac{\frac{d_2}{1 + \delta_2^{\alpha}} - \frac{d_1}{1 + \delta_1^{\alpha}}}{\frac{1 + \delta_2^{\beta}}{1 + \delta_2^{\alpha}} - \frac{1 + \delta_1^{\beta}}{1 + \delta_1^{\alpha}}} = \frac{\frac{d_2}{1 + \delta_2^{\alpha}} - \frac{d_1}{1 + \delta_1^{\alpha}}}{\frac{\delta_1^{\text{sp}}}{1 + \delta_1^{\alpha}} - \frac{\delta_2^{\text{sp}}}{1 + \delta_2^{\alpha}}} \quad (23a)$$

$$\begin{aligned}
\gamma &= \frac{\frac{d_2}{1+\delta_2^\alpha} \left(\frac{1+\delta_1^\beta}{1+\delta_1^\alpha} \right) - \frac{d_1}{1+\delta_1^\alpha} \left(\frac{1+\delta_2^\beta}{1+\delta_2^\alpha} \right)}{\frac{1+\delta_2^\beta}{1+\delta_2^\alpha} - \frac{1+\delta_1^\beta}{1+\delta_1^\alpha}} \\
&= \frac{\frac{d_2}{1+\delta_2^\alpha} \left(\frac{1+\delta_1^\beta}{1+\delta_1^\alpha} \right) - \frac{d_1}{1+\delta_1^\alpha} \left(\frac{1+\delta_2^\beta}{1+\delta_2^\alpha} \right)}{\frac{\delta_1^{\text{sp}}}{1+\delta_1^\alpha} - \frac{\delta_2^{\text{sp}}}{1+\delta_2^\alpha}}
\end{aligned} \tag{23b}$$

The denominators of these expressions can be approximated by the difference $\delta_1^{\text{sp}} - \delta_2^{\text{sp}}$. Thus, if the site preferences of the reference gases are similar, the value of the denominator approaches zero and the solutions will become uncertain due to the finite measurement error. Then, the question arises, how far apart must the site preferences of the reference materials be to obtain robust solutions?

The general form of uncertainty propagation in a variable a with respect to the observations (y_i) is given by the following equation⁷²:

$$\sigma_a^2 = \sum_i \sigma_i^2 \left(\frac{\partial a}{\partial y_i} \right)^2$$

where σ_a is the uncertainty in a , y_i is an individual observation, and σ_i is the uncertainty in the observation y_i . Ignoring the uncertainties in ^{45}R and the assigned position-dependent ^{15}R values, the uncertainty in κ can be calculated as:

$$\sigma_\kappa^2 = \sigma_{^{31}\text{R}_1}^2 \left(\frac{\partial \kappa}{\partial ^{31}\text{R}_1} \right)^2 + \sigma_{^{31}\text{R}_2}^2 \left(\frac{\partial \kappa}{\partial ^{31}\text{R}_2} \right)^2$$

$$\begin{aligned}
\frac{\partial \kappa}{\partial ^{31}\text{R}_1} &= \frac{\frac{-(1+^{15}\text{R}_1^\alpha)(1+^{15}\text{R}_1^\beta)}{^{15}\text{R}_1^\alpha(1+^{15}\text{R}_1^\alpha+^{15}\text{R}_1^\beta+^{31}\text{R}_1-^{45}\text{R}_1)^2}}{\frac{\delta_1^{\text{sp}}}{1+\delta_1^\alpha} - \frac{\delta_2^{\text{sp}}}{1+\delta_2^\alpha}} \approx \frac{-1}{^{15}\text{R}_1^\alpha(\delta_1^{\text{sp}} - \delta_2^{\text{sp}})} \\
\frac{\partial \kappa}{\partial ^{31}\text{R}_2} &= \frac{\frac{-(1+^{15}\text{R}_2^\alpha)(1+^{15}\text{R}_2^\beta)}{^{15}\text{R}_2^\alpha(1+^{15}\text{R}_2^\alpha+^{15}\text{R}_2^\beta+^{31}\text{R}_2-^{45}\text{R}_2)^2}}{\frac{\delta_1^{\text{sp}}}{1+\delta_1^\alpha} - \frac{\delta_2^{\text{sp}}}{1+\delta_2^\alpha}} \approx \frac{-1}{^{15}\text{R}_2^\alpha(\delta_1^{\text{sp}} - \delta_2^{\text{sp}})}
\end{aligned}$$

Assuming $\sigma_{^{31}\text{R}}/^{15}\text{R}^\alpha = \sigma_{^{31}\text{R}_1}/^{15}\text{R}_1^\alpha = \sigma_{^{31}\text{R}_2}/^{15}\text{R}_2^\alpha$, then

$$\sigma_\kappa^2 \approx 2 \left(\frac{\sigma_{^{31}\text{R}}}{^{15}\text{R}^\alpha} \right)^2 \left(\frac{1}{\delta_1^{\text{sp}} - \delta_2^{\text{sp}}} \right)^2$$

or

$$\sigma_\kappa \approx \sqrt{2} \frac{\sigma(^{31}\text{R})}{^{15}\text{R}^\alpha} \frac{1}{|\delta_1^{\text{sp}} - \delta_2^{\text{sp}}|} \tag{24a}$$

437 Similarly, for γ :

$$\sigma_\gamma \approx \sqrt{2} \frac{\sigma(^{31}R)}{{}^{15}R^\beta} \frac{1}{|\delta_1^{\text{sp}} - \delta_2^{\text{sp}}|} \quad (24b)$$

438 where $\sigma(^{31}R)/{}^{15}R$ can be approximated by the measurement uncertainty in $^{31}\delta$ and
 439 $|\delta_1^{\text{sp}} - \delta_2^{\text{sp}}|$ is the absolute value of the difference in assigned site preferences between the two
 440 reference materials. This means that for a measurement uncertainty in $^{31}\delta$ of 1 ‰ and a $\delta(^{15}\text{N}^{\text{sp}})$
 441 difference of 10 ‰ between the two reference materials, γ and κ would have absolute
 442 uncertainties of 0.14. This uncertainty translates into a relative uncertainty of about 30 % for the
 443 $\delta(^{15}\text{N}^{\text{sp}})$ value of an unknown sample – far too high for practical applications (Supplementary
 444 text S4). A $\delta(^{15}\text{N}^{\text{sp}})$ difference of 100 ‰ would give a more useful absolute uncertainty of 0.014
 445 for γ and κ .

446 These theoretical uncertainties are reflected in the experimental data. For Lab 1, the
 447 reference materials 53504 ($\delta(^{15}\text{N}^{\text{sp}}) = -92.73$ ‰) and CA08214 ($\delta(^{15}\text{N}^{\text{sp}}) = 20.54$ ‰) yielded $\gamma =$
 448 0.174 ± 0.022 and $\kappa = 0.083 \pm 0.022$. The standard deviation of $^{31}\delta$ was 1.89 ‰ ($n = 12$). This
 449 produces an estimated uncertainty in γ and κ of $\sqrt{2}(1.89 \text{ ‰})/(113.27 \text{ ‰}) = 0.024$, which agrees
 450 well with the experimental data. Similarly, reference materials 53504 and CA06261 ($\delta(^{15}\text{N}^{\text{sp}}) =$
 451 27.07 ‰) yielded $\gamma = 0.163 \pm 0.018$ and $\kappa = 0.073 \pm 0.018$. The standard deviation of $^{31}\delta$ was 1.58
 452 ‰ ($n = 10$), and the $\delta(^{15}\text{N}^{\text{sp}})$ difference was 119.80 ‰. This produced an estimated uncertainty in
 453 γ and κ of $\sqrt{2}(1.58 \text{ ‰})/(119.80 \text{ ‰}) = 0.019$, also in line with the uncertainties in γ and κ .

454 Rearranging eqns. (24a) and (24b), we obtain expressions for the required $|\delta_1^{\text{sp}} - \delta_2^{\text{sp}}|$ to
 455 obtain a target level of uncertainty (σ) in γ and κ , given the measurement uncertainty in ^{31}R :

$$|\delta_1^{\text{sp}} - \delta_2^{\text{sp}}| = \sqrt{2} \frac{\sigma(^{31}R)}{{}^{15}R^\alpha} \frac{1}{\sigma_\kappa} \quad (25a)$$

456

$$|\delta_1^{\text{sp}} - \delta_2^{\text{sp}}| = \sqrt{2} \frac{\sigma(^{31}R)}{{}^{15}R^\beta} \frac{1}{\sigma_\gamma} \quad (25b)$$

457 Assuming $\sigma(^{31}R)/{}^{15}R^\alpha \approx \sigma(^{31}R)/{}^{15}R^\beta \approx \sigma(^{31}\delta)$, we obtain:

$$|\delta_1^{\text{sp}} - \delta_2^{\text{sp}}| = \sqrt{2} \sigma(^{31}\delta) \frac{1}{\sigma_{\gamma\kappa}} \quad (26)$$

458

459 where $\sigma(^{31}\delta)$ is the $^{31}\delta$ measurement uncertainty in per mil, and $\sigma_{\gamma\kappa}$ is the target absolute
 460 uncertainty in γ and κ . For example, with a measurement uncertainty of 1 ‰ in $^{31}\delta$, the $\delta(^{15}\text{N}^{\text{sp}})$
 461 values of the two reference materials must differ by at least 141 ‰ to achieve an absolute
 462 uncertainty in γ and κ of 0.01. Based on these results, we recommend calculating γ and κ from
 463 reference materials with a large $\delta(^{15}\text{N}^{\text{sp}})$ difference, as estimated from eqn. (26).

464 As an alternative to the algebraic solution, a least squares optimization can be used to
 465 find a solution for γ and κ , although that solution may find a local optimum rather than a global
 466 optimum. The user can select a least squares optimization instead of the algebraic solution with
 467 the “method” keyword argument to pyisotopomer’s Scrambling function. The least squares
 468 optimization smooths measurement uncertainty, making it useful for fitting repeat

measurements of reference materials to a single pair of "best" values for γ and κ . Its disadvantage is that, unlike the algebraic solution, the least squares optimization depends on the initial guess for γ and κ . Using data from reference materials CA06261 and CA08214, a range of initial guesses from $\gamma = \kappa = 0.000$ to $\gamma = \kappa = 0.200$ produced a range of least squares solutions, from $\gamma = 0.090$ and $\kappa = 0.000$ to $\gamma = 0.269$ and $\kappa = 0.183$ (Figure S3). Despite this range of γ and κ , however, the least squares optimization produced a consistent $\gamma - \kappa$ of 0.09. As shown in Section 4.4, $\gamma - \kappa$ governs the accuracy of $\delta(^{15}\text{N}^{\text{sp}})$ far more than the individual values of γ and κ .

Given an accurate initial guess, the least squares optimization will find a minimum at or close to this initial guess, even for reference material pairings close in their $\delta(^{15}\text{N}^{\text{sp}})$. For example, when we used the algebraic γ and κ from reference materials CA08214 and 53504 as an initial guess, the least squares optimization produced similar γ and κ for a variety of reference material pairings (Table S2). Furthermore, for the same initial guess, the least squares optimization finds different solutions for the Lab 1 and Lab 2 instruments, even for reference material pairings close in their $\delta(^{15}\text{N}^{\text{sp}})$ (Table S3). This demonstrates that, depending on the measurement precision at the time, the least squares optimization searches an appropriately wide solution space to resolve large differences in instrument behavior.

If the first-time user wishes to obtain accurate individual values of γ and κ , we recommend obtaining reference materials different enough in their $\delta(^{15}\text{N}^{\text{sp}})$ to calculate γ and κ with the algebraic solution. If the user wishes to take advantage of the smoothing of the least squares optimization, this algebraic γ and κ can then be used as the initial guess for the least squares solver.

We also recommend that the user test the accuracy of the least squares γ and κ by plugging γ and κ back into eqn. (10) and comparing the result to the measured ^{31}R for each reference material. The two ^{31}R values should match. pyisotopomer performs this calculation automatically and outputs the difference as a δ value:

$$^{31}\delta_{\text{error}} = \frac{^{31}\text{R}_{\text{calculated}}}{^{31}\text{R}_{\text{measured}}} - 1 \quad (27)$$

where $^{31}\text{R}_{\text{calculated}}$ is calculated by plugging the least squares γ and κ into eqn. (10), and $^{31}\text{R}_{\text{measured}}$ represents the measured ^{31}R for each reference material. In the intercalibration exercise, the mean of the absolute values of $^{31}\delta_{\text{error}}$ from least squares γ and κ solutions ranged from 0.27 ‰ to 0.86 ‰ (Table S2), similar in magnitude to the $^{31}\delta$ analytical uncertainty for Labs 1 and 2 (Table S5). This indicates that the amount of error introduced by using the least squares optimization is similar to the measurement error in $^{31}\delta$. In comparison, the $^{31}\delta_{\text{error}}$ introduced by the algebraic solution corresponded to values of $(^{31}\text{R}_{\text{calculated}} - ^{31}\text{R}_{\text{measured}})$ within machine precision (Table S2).

4.3 Variability in fragmentation behavior

As shown above, $\gamma - \kappa$, as opposed to the individual values of γ and κ , is the best constrained parameter in the scrambling calculation. We show below that $\gamma - \kappa$ also has the greatest impact on $\delta(^{15}\text{N}^{\alpha})$, $\delta(^{15}\text{N}^{\beta})$, and $\delta(^{15}\text{N}^{\text{sp}})$. $\gamma - \kappa$ is proportional to $^{31}\delta - ^{45}\delta$, and thus is a metric of an instrument's scrambling behavior.

To examine the change in the fragmentation behavior of a single IRMS over time, we compiled values of $\gamma - \kappa$ for Lab 1 from June 2018 – March 2021 (Figure 3). To equally weigh

each day of running the instrument, first, we calculated a daily mean $\gamma - \kappa$, then calculated a five-day running average of $\gamma - \kappa$ from these daily means. The value of $\gamma - \kappa$ varied throughout the time series, with a mean of 0.092 ± 0.002 . High volatility in $\gamma - \kappa$ in February-April 2019 corresponded with a period when the lab temperature was poorly controlled, with strong day-night variation (Figure 3). During periods when the lab temperature was stable, $\gamma - \kappa$ tended to increase as the instrument box and trap currents diverged with filament age, although no linear relationship emerged

There are several reasons why the scrambling behavior of the ion source might change over time. The NO^+ fragment ion can be produced by one of several routes from N_2O^+ ^{73,74}. The pathways and associated isotope effects for the formation of fragment ions are affected by collision frequency, the distribution of excited states, and the time spent in the ion source, which suggests that ion source conditions such as vapor pressure, ionizing energy, and accelerating voltage may all influence the fragmentation behavior of an IRMS system^{54,73–76}. For these reasons, performing the scrambling calibration only once is insufficient to obtain high-quality N_2O isotopocule data. Instead, it is important to recalibrate an IRMS system for scrambling on a regular basis since ion source conditions may change with time and can shift abruptly with events such as filament changes. We recommend using a running average of γ and κ over a window corresponding to 10 pairings of reference materials, corresponding to a five-day window if two pairs of reference materials are run per day. If there is high volatility in γ and κ , as seen above in March-April 2019, it may be necessary to shorten this window, to apply scrambling corrections most appropriate to instrument conditions.

4.4 Sensitivity of position-dependent δ values to uncertainty in scrambling coefficients

The uncertainty in $\delta(^{15}\text{N}^\alpha)$, $\delta(^{15}\text{N}^\beta)$, and $\delta(^{15}\text{N}^{\text{sp}})$ associated with the uncertainty in each scrambling coefficient is less straightforward to assess than the uncertainty in ^{31}R given by eqns. (23) and (24), due to the nonlinear relationship between $\delta(^{15}\text{N}^\alpha)$, $\delta(^{15}\text{N}^\beta)$, γ , and κ : (see eqn. (53) of Kaiser and Röckmann, 2008). A first order approximation of $\delta(^{15}\text{N}^{\text{sp}})$ is given by (supplementary text S4):

$$\delta(^{15}\text{N}^{\text{sp}}) \approx \frac{2(1 - \gamma + \kappa)}{1 - \gamma - \kappa} ({}^{31}\delta - {}^{45}\delta) \quad (28)$$

From this equation, it is apparent that $\delta(^{15}\text{N}^{\text{sp}})$ is modulated primarily by the difference $\gamma - \kappa$, rather than the individual values of γ and κ . It is also apparent that $\gamma - \kappa$ is proportional to ${}^{31}\delta - {}^{45}\delta$.

A Monte Carlo simulation can be a useful way of visualizing how γ , κ , and, $\gamma - \kappa$ impact $\delta(^{15}\text{N}^\alpha)$, $\delta(^{15}\text{N}^\beta)$, and $\delta(^{15}\text{N}^{\text{sp}})$. We performed two sensitivity experiments with data from Lab 1:

- 1) sensitivity of $\delta(^{15}\text{N}^\alpha)$, $\delta(^{15}\text{N}^\beta)$, and $\delta(^{15}\text{N}^{\text{sp}})$ to $\gamma - \kappa$;
- 2) sensitivity of $\delta(^{15}\text{N}^\alpha)$, $\delta(^{15}\text{N}^\beta)$, and $\delta(^{15}\text{N}^{\text{sp}})$ to the individual values of γ and κ , holding their difference constant.

For the first sensitivity experiment, a Monte Carlo simulation was used to introduce random uncertainty in the γ and κ values used to calculate δ values of three reference materials. Based Table S2, we chose $\gamma = 0.174$ and $\kappa = 0.083$ as central values and varied $\gamma - \kappa$ such that the standard deviation of $\gamma - \kappa$ was equal to 10 % of the mean (0.091). For the second sensitivity experiment, we modeled γ and κ in tandem as random numbers centered around $\gamma = 0.174$ and $\kappa = 0.083$, with uncertainties equal to 10 % of the mean γ , and held $\gamma - \kappa$ constant at 0.091. For both experiments, we sampled 1000 pairs of γ and κ , and then calculated the 1000 simulated

values of $\delta(^{15}\text{N}^\alpha)$, $\delta(^{15}\text{N}^\beta)$, and $\delta(^{15}\text{N}^\text{sp})$ for the three reference materials (CA06261, 53504, CA08214).

This analysis showed that a 10 % relative uncertainty in $\gamma - \kappa$ can lead to large variations in $\delta(^{15}\text{N}^\alpha)$, $\delta(^{15}\text{N}^\beta)$, and $\delta(^{15}\text{N}^\text{sp})$, e.g., pooled standard deviations of 17.1-18.5 ‰ for $\delta(^{15}\text{N}^\text{sp})$ (Figure 4a-c). In contrast, a 10 % relative error in γ , keeping $\gamma - \kappa$ constant, led to pooled standard deviations of 1.0-4.3 ‰ in $\delta(^{15}\text{N}^\text{sp})$ (Figure 4d-f). In both experiments, varying γ and κ produced the most variability for reference material 53504, whose $\delta(^{15}\text{N}^\text{sp})$ was greatest in magnitude.

These results reflect the earlier conclusion that $\gamma - \kappa$ is the best constrained parameter in the scrambling calculation, and, conversely, that this difference has the greatest effect on $\delta(^{15}\text{N}^\text{sp})$. Thus, we recommend regular scrambling calibrations, as assuming the wrong $\gamma - \kappa$ difference may have a significant impact on site preferences calculated from these coefficients.

4.5 Comparison of results between two IRMS laboratories

The application of pyisotopomer was tested through an intercalibration including four reference materials and two Lake Lugano samples measured by two IRMS laboratories, plus two additional reference materials run in Lab 1. Using an average γ and κ produced by the algebraic method from the pairing of reference materials 53504 and CA08214, isotopomers were calculated for lake water unknowns, four reference materials run as unknowns for quality control, and the two reference materials used in the calibration and (Table 2). This exercise was repeated, calculating γ and κ instead with least squares method and the pairing of reference materials CA06261 and CA08214 (Table S4). The root mean square deviation (RMSD) for each reference material was calculated by comparison to the calibrated values provided by a previous intercalibration effort⁵⁶ (for atmosphere-equilibrated seawater), an internal standard (B6), and for gases sourced from J. Mohn (S2, CA06261, 53504, and CA08214). Almost all isotopomer values produced by the least squares optimization (Table S4) were within error of those produced by the algebraic solution (Table 2); the latter is discussed below.

The $\delta(^{15}\text{N}^\text{bulk})$ measured by the two labs displayed good agreement for each of the four reference materials, as well as the lake water samples. The $\delta(^{15}\text{N}^\text{bulk})$ RMSDs ranged from 0.2 to 0.6 ‰ (Table 2), all of which were smaller than the 0.8 ‰ presented for IRMS labs by Mohn et al., (2014). The RMSD for atmospheric N_2O was highest, at 0.6 ‰. For both lake water samples, the $\delta(^{15}\text{N}^\text{bulk})$ values measured by Lab 1 and Lab 2 were statistically indistinguishable (Table 2; Figure S4). Likewise, the $\delta(^{18}\text{O})$ measured by the two labs displayed good agreement for each of the four reference materials measured by both labs, as well as the lake water samples. The $\delta(^{18}\text{O})$ RMSDs were slightly greater than the 1.00 ‰ presented for IRMS labs by Mohn et al. (2014), ranging from 0.5 ‰–1.7 ‰, with the greatest RMSD for reference material 53504 (Table 2). For the lake water unknowns, the $\delta(^{18}\text{O})$ values measured by the two labs were within error of each other (Table 2; Figure S4).

The $\delta(^{15}\text{N}^\alpha)$ measured by the two labs also showed good agreement for reference materials CA06261, CA08214, and atmosphere-equilibrated seawater: in each case, the combined RMSD was less than 2.4 ‰ (Table 2). This is similar to the data presented in Mohn et al. (2014), who find an RMSD for $\delta(^{15}\text{N}^\alpha)$ for IRMS laboratories of 2.47 ‰. The $\delta(^{15}\text{N}^\alpha)$ measured by Lab 1 for reference material 53504 (0.0 ± 1.0 ‰) was lower than both the calibrated value (1.71 ‰) and the value measured by Lab 2 (1.7 ± 1.0 ‰). The values of $\delta(^{15}\text{N}^\alpha)$ measured by the two labs for the two lake water samples, however, were within error of each other. For $\delta(^{15}\text{N}^\beta)$, the RMSDs for each reference material were of a similar order of magnitude to $\delta(^{15}\text{N}^\alpha)$,

ranging from 0.2 ‰-2.1 ‰, similar to the value 2.12 ‰ reported by Mohn et al. (2014). The $\delta(^{15}\text{N}^\beta)$ measured by Lab 1 for the lake water unknowns was within error of that measured by Lab 2 (Table 2; Figure S4). Of note, the $\delta(^{15}\text{N}^\beta)$ for the lake water unknown taken at 90 m depth was -32.8 ‰ (average of measurements by Lab 1 and Lab 2), which is far more negative than most values observed previously^{26,31}.

The $\delta(^{15}\text{N}^{\text{sp}})$ values measured by the two laboratories showed larger standard deviations than the $\delta(^{15}\text{N}^\alpha)$ and $\delta(^{15}\text{N}^\beta)$ individually, which is to be expected, since $\delta(^{15}\text{N}^{\text{sp}})$ is a measure of difference between the latter two parameters. The $\delta(^{15}\text{N}^{\text{sp}})$ RMSD values, however, were all less than 3 ‰ for atmosphere-equilibrated seawater, 53504, and CA08214 (Table 2). This represents an improvement on Mohn et al. (2014), who find an RMSD of 4.29 ‰ for $\delta(^{15}\text{N}^{\text{sp}})$ measured by IRMS laboratories. The $\delta(^{15}\text{N}^{\text{sp}})$ RMSD for reference material CA06261 was greater, at 4.4 ‰, which may result from this reference material having a more negative $\delta(^{15}\text{N}^\alpha)$ than either of the two reference materials used in the scrambling calibration. The lake water samples showed larger offsets in $\delta(^{15}\text{N}^{\text{sp}})$ than the reference materials (Figure S4). The lake water sample from 10 m depth showed an especially large difference in $\delta(^{15}\text{N}^{\text{sp}})$ between Lab 1 and Lab 2: Lab 1 measured a mean $\delta(^{15}\text{N}^{\text{sp}})$ of (18.8 ± 1.6) ‰ at this depth, while Lab 2 measured a mean $\delta(^{15}\text{N}^{\text{sp}})$ of (21.4 ± 2.5) ‰ (Table 2). At 90 m depth, Lab 1 measured a mean $\delta(^{15}\text{N}^{\text{sp}})$ of 52.3 ± 1.2 ‰, and Lab 2 measured a mean $\delta(^{15}\text{N}^{\text{sp}})$ of (50.9 ± 0.5) ‰.

After size correction and scale normalization, the only consistent difference between measurements made by the two labs were differences in peak area, which may reflect differences in the setup of the purge and trap system and/or differences in instrument sensitivity. The N_2O amounts measured in the lake water samples, however, were also similar between the two labs involved in the intercalibration exercise, indicating that this difference in sensitivity was adequately compensated for by the peak area to amount conversion factor. In the sample taken at 10 m depth, Lab 1 found (2.97 ± 0.04) nmol; Lab 2 found (2.31 ± 0.09) nmol. At 90 m depth, Lab 1 found (20.46 ± 0.37) nmol; Lab 2 found (19.82 ± 0.01) nmol N_2O . All bottle volumes were the same. Thus, we conclude that differences in sample pretreatment procedure were corrected for by the size correction and scale normalization steps, leaving no residual effect on the final δ values or N_2O amounts.

4.6 Additional considerations

The pyisotopomer package produces good results if each of the data preprocessing steps properly account for size- and delta-dependent effects on the measured isotope ratios $^{31}\delta$, $^{45}\delta$, and $^{46}\delta$. However, it will produce spurious results under the following circumstances. Firstly, varying blanks may introduce errors due to the size correction not being applicable to samples and reference materials alike. Second, if the $^{45}\delta$ and $^{46}\delta$ scale normalization slope and intercept differ substantially from one and zero (such as a negative slope), there likely exists an issue with the scale normalization (such as the reference materials not spanning a wide enough range in $^{45}\delta$ and $^{46}\delta$). A spurious scale normalization will likewise produce errors in the final isotopocule values. Thirdly, if reference materials that are too close in their site preferences are used to determine γ and κ with the algebraic solution, the resulting coefficients may represent "unphysical" values (i.e., not between 0 and 1); these, however, would be inconsequential if the unknown samples have $\delta(^{15}\text{N}^{\text{sp}})$ values close to these reference materials. Finally, $\delta(^{17}\text{O})$ is calculated from a mass dependent relationship with $\delta(^{18}\text{O})$ (the parameters of which can be adjusted with keyword arguments to the Scrambling and Isotopomers functions) unless $\Delta(^{17}\text{O})$ is determined separately^{59,61,62} and entered in the data corrections template.

5. Conclusion: How to obtain high-quality N₂O isotopocule data using pyisotopomer

Using pyisotopomer and three reference materials, one can characterize the scrambling behavior for a given IRMS and apply those scrambling coefficients to calculate the isotopocule values of unknown samples. To ensure high-quality results from these calculations, we provide the following recommendations. Firstly, if reference materials with suitably distinct site preferences are available, we recommend calculating the scrambling coefficients γ and κ from algebraic solution of eqns. (11) and (12), which is the default method in the Scrambling function of pyisotopomer. We offer the least squares approach as an alternative, with the following caveats: 1) The least squares solver finds a minimum close to the initial guess for γ and κ . As such, if the solver is fed an initial guess other than the absolute minimum calculated from the algebraic solution, it will find the “wrong” absolute value of γ and κ . It will, however, find the correct value of $\gamma - \kappa$, which has a much larger impact on calculated isotopocules. 2) Using the “wrong” scrambling coefficients will have only a small effect if the unknowns are close in their $\delta(^{15}\text{N}^\alpha)$, $\delta(^{15}\text{N}^\beta)$, and $\delta(^{15}\text{N}^{\text{sp}})$ to those of the reference materials but will have a deleterious effect as the unknowns diverge in their isotopomer values from the reference materials. 3) If an initial guess is available, such as through a calibration with the algebraic solution, this should be used as the initial guess for the least squares solver. Otherwise, we recommend iterating through the scrambling calculation twice. Use the solution from the first iteration as the initial guess for subsequent calculations. 4) It is necessary to run paired reference materials daily to obtain accurate running estimates of γ and κ . It is recommended to convert these daily estimates to a one-week running average and use that average to calculate the isotopocules of unknown samples.

Using pyisotopomer in an intercalibration exercise and implementing the above recommendations, we find good agreement between the calibrated δ values measured by two different IRMS labs for both reference materials and natural lake samples. We conclude that while the intercalibration results demonstrate potential for further improvement in precision, the intercalibration of $\delta(^{15}\text{N}^{\text{sp}})$ using a uniform scrambling calculation (pyisotopomer) presented here represents an improvement upon previous N₂O intercalibrations.

Data availability statement

The manuscript is prepared to comply with the RCMS data policy. The latest version of pyisotopomer is available for installation via the Python Package index (pypi.org/project/pyisotopomer). The second release of pyisotopomer is also available via Zenodo (doi.org/10.5281/zenodo.7552724). This research was supported by U.S.-NSF grant OCE-1657868 to K. L. Casciotti. C. L. Kelly is supported by an NSF Graduate Research Fellowship. The authors declare no competing financial interests.

References

1. Yung YL, Wang WC, Lacis AA. Greenhouse effect due to atmospheric nitrous oxide. *Geophys Res Lett*. 1976;3(10):619-621. doi:10.1029/GL003i010p00619
2. Smith C, Nicholls ZRJ, Armour K, et al. The Earth's Energy Budget, Climate Feedbacks, and Climate Sensitivity Supplementary Material. In: Masson-Delmotte V, Zhai P, Pirani A, et al., eds. *Climate Change 2021: The Physical Science Basis. Contribution of Working Group I to the Sixth Assessment Report of the Intergovernmental Panel on Climate Change*. Cambridge University Press; 2021. Accessed October 4, 2021. https://www.ipcc.ch/report/ar6/wg1/downloads/report/IPCC_AR6_WGI_Chapter_07_Supplementary_Material.pdf
3. Crutzen PJ. The influence of nitrogen oxides on the atmospheric ozone content. *Q J R Meteorol Soc*. 1970;96(408):320-325. doi:10.1002/qj.49709640815
4. Ravishankara AR, Daniel JS, Portmann RW. Nitrous Oxide (N₂O): The Dominant Ozone-Depleting Substance Emitted in the 21st Century. *Science*. 2009;326(5949):123-125. doi:10.1126/science.1176985
5. Wuebbles DJ. Nitrous Oxide: No Laughing Matter. *Science*. 2009;326(5949):56-57. doi:10.1126/science.1179571
6. Müller R. The impact of the rise in atmospheric nitrous oxide on stratospheric ozone. *Ambio*. 2021;50(1):35-39. doi:10.1007/s13280-020-01428-3
7. Kim KR, Craig H. Nitrogen-15 and Oxygen-18 Characteristics of Nitrous Oxide: A Global Perspective. *Science*. 1993;262(5141):1855-1857. doi:10.1126/science.262.5141.1855
8. Pérez T, Trumbore SE, Tyler SC, Davidson EA, Keller M, Camargo PB de. Isotopic variability of N₂O emissions from tropical forest soils. *Glob Biogeochem Cycles*. 2000;14(2):525-535. doi:10.1029/1999GB001181
9. Kim KR, Craig H. Two-isotope characterization of N₂O in the Pacific Ocean and constraints on its origin in deep water. *Nature*. 1990;347(6288):58-61. doi:10.1038/347058a0
10. Dore JE, Popp BN, Karl DM, Sansone FJ. A large source of atmospheric nitrous oxide from subtropical North Pacific surface waters. *Nature*. 1998;396(6706):63-66. doi:10.1038/23921
11. Naqvi SWA, Naik H, Jayakumar A, et al. Seasonal Anoxia Over the Western Indian Continental Shelf. In: Wiggert JD, Hood RR, Naqvi SWA, Brink KH, Smith SL, eds. *Geophysical Monograph Series*. Vol 185. American Geophysical Union; 2009:333-345. doi:10.1029/2008GM000745
12. Yoshida N, Hattori A, Saino T, Matsuo S, Wada E. 15N/14N ratio of dissolved N₂O in the eastern tropical Pacific Ocean. *Nature*. Published online 1984. doi:10.1038/307442A0

- 720 13. Rahn T, Wahlen M. Stable Isotope Enrichment in Stratospheric Nitrous Oxide. *Science*.
721 1997;278(5344):1776-1778. doi:10.1126/science.278.5344.1776
- 722 14. Rahn T, Wahlen M. A reassessment of the global isotopic budget of atmospheric nitrous
723 oxide. *Glob Biogeochem Cycles*. 2000;14(2):537-543. doi:10.1029/1999GB900070
- 724 15. Yoshida N. ¹⁵N-depleted N₂O as a product of nitrification. *Nature*. 1988;335(6190):528-
725 529. doi:10.1038/335528a0
- 726 16. Barford CC, Montoya JP, Altabet MA, Mitchell R. Steady-State Nitrogen Isotope Effects of
727 N₂ and N₂O Production in *Paracoccus denitrificans*. *Appl Environ Microbiol*.
728 1999;65(3):989-994. doi:10.1128/AEM.65.3.989-994.1999
- 729 17. Pérez T, Trumbore SE, Tyler SC, et al. Identifying the agricultural imprint on the global
730 N₂O budget using stable isotopes. *J Geophys Res Atmospheres*. 2001;106(D9):9869-9878.
731 doi:10.1029/2000JD900809
- 732 18. Yamulki S, Toyoda S, Yoshida N, Veldkamp E, Grant B, Bol R. Diurnal fluxes and the
733 isotopomer ratios of N₂O in a temperate grassland following urine amendment. *Rapid*
734 *Commun Mass Spectrom*. 2001;15(15):1263-1269. doi:10.1002/rcm.352
- 735 19. Lewicka-Szczebak D, Augustin J, Gieseemann A, Well R. Quantifying N₂O reduction to N₂
736 based on N₂O isotopocules – validation with independent methods (helium incubation and
737 ¹⁵N gas flux method). *Biogeosciences*. 2017;14(3):711-732. doi:https://doi.org/10.5194/bg-
738 14-711-2017
- 739 20. Verhoeven E, Barthel M, Yu L, et al. Early season N₂O emissions under variable water
740 management in rice systems: source-partitioning emissions using isotope ratios along a
741 depth profile. *Biogeosciences*. 2019;16(2):383-408. doi:https://doi.org/10.5194/bg-16-383-
742 2019
- 743 21. Yoshida N, Toyoda S. Constraining the atmospheric N₂O budget from intramolecular site
744 preference in N₂O isotopomers. *Nature*. 2000;405(6784):330-334. doi:10.1038/35012558
- 745 22. Prokopiou M, Martinerie P, [Link to external site this link will open in a new window](#), et al.
746 Constraining N₂O emissions since 1940 using firn air isotope measurements in both
747 hemispheres. *Atmospheric Chem Phys*. 2017;17(7):4539-4564. doi:10.5194/acp-17-4539-
748 2017
- 749 23. Yu L, Harris E, Henne S, et al. The isotopic composition of atmospheric nitrous oxide
750 observed at the high-altitude research station Jungfraujoch, Switzerland. *Atmospheric Chem*
751 *Phys*. 2020;20(11):6495-6519. doi:10.5194/acp-20-6495-2020
- 752 24. Toyoda S, Yoshida N, Miwa T, et al. Production mechanism and global budget of N₂O
753 inferred from its isotopomers in the western North Pacific. *Geophys Res Lett*. 2002;29(3):7-
754 1-7-4. doi:10.1029/2001GL014311

- 755 25. Popp BN, Westley MB, Toyoda S, et al. Nitrogen and oxygen isotopomeric constraints on
756 the origins and sea-to-air flux of N₂O in the oligotrophic subtropical North Pacific gyre.
757 *Glob Biogeochem Cycles*. 2002;16(4):12-1-12-10. doi:10.1029/2001GB001806
- 758 26. Yamagishi H, Westley MB, Popp BN, et al. Role of nitrification and denitrification on the
759 nitrous oxide cycle in the eastern tropical North Pacific and Gulf of California. *J Geophys*
760 *Res Biogeosciences*. 2007;112(G2). doi:10.1029/2006JG000227
- 761 27. Yamagishi H, Yoshida N, Toyoda S, Popp BN, Westley MB, Watanabe S. Contributions of
762 denitrification and mixing on the distribution of nitrous oxide in the North Pacific. *Geophys*
763 *Res Lett*. 2005;32(4). doi:10.1029/2004GL021458
- 764 28. Westley MB, Yamagishi H, Popp BN, Yoshida N. Nitrous oxide cycling in the Black Sea
765 inferred from stable isotope and isotopomer distributions. *Deep Sea Res Part II Top Stud*
766 *Oceanogr*. 2006;53(17-19):1802-1816. doi:10.1016/j.dsr2.2006.03.012
- 767 29. Farías L, Castro-González M, Cornejo M, et al. Denitrification and nitrous oxide cycling
768 within the upper oxycline of the eastern tropical South Pacific oxygen minimum zone.
769 *Limnol Oceanogr*. 2009;54(1):132-144. doi:10.4319/lo.2009.54.1.0132
- 770 30. Casciotti KL, Forbes M, Vedamati J, Peters BD, Martin TS, Mordy CW. Nitrous oxide
771 cycling in the Eastern Tropical South Pacific as inferred from isotopic and isotopomeric
772 data. *Deep Sea Res Part II Top Stud Oceanogr*. 2018;156:155-167.
773 doi:10.1016/j.dsr2.2018.07.014
- 774 31. Bourbonnais A, Letscher RT, Bange HW, et al. N₂O production and consumption from
775 stable isotopic and concentration data in the Peruvian coastal upwelling system. *Glob*
776 *Biogeochem Cycles*. 2017;31(4):678-698. doi:10.1002/2016GB005567
- 777 32. Toyoda S, Yoshida O, Yamagishi H, Fujii A, Yoshida N, Watanabe S. Identifying the
778 origin of nitrous oxide dissolved in deep ocean by concentration and isotopocule analyses.
779 *Sci Rep*. 2019;9(1):1-9. doi:10.1038/s41598-019-44224-0
- 780 33. Kelly CL, Travis NM, Baya PA, Casciotti KL. Quantifying Nitrous Oxide Cycling Regimes
781 in the Eastern Tropical North Pacific Ocean With Isotopomer Analysis. *Glob Biogeochem*
782 *Cycles*. 2021;35(2):e2020GB006637. doi:10.1029/2020GB006637
- 783 34. Toyoda S, Kakimoto T, Kudo K, et al. Distribution and Production Mechanisms of N₂O in
784 the Western Arctic Ocean. *Glob Biogeochem Cycles*. 2021;35(4):e2020GB006881.
785 doi:https://doi.org/10.1029/2020GB006881
- 786 35. Friedman L, Bigeleisen J. Oxygen and Nitrogen Isotope Effects in the Decomposition of
787 Ammonium Nitrate. *J Chem Phys*. 1950;18(10):1325-1331. doi:10.1063/1.1747471
- 788 36. Toyoda S, Yoshida N. Determination of nitrogen isotopomers of nitrous oxide on a
789 modified isotope ratio mass spectrometer. *Anal Chem*. 1999;71(20):4711-4718.
790 doi:10.1021/ac9904563

- 791 37. Brenninkmeijer CAM, Röckmann T. Mass spectrometry of the intramolecular nitrogen
792 isotope distribution of environmental nitrous oxide using fragment-ion analysis. *Rapid*
793 *Commun Mass Spectrom.* 1999;13(20):2028-2033. doi:10.1002/(SICI)1097-
794 0231(19991030)13:20<2028::AID-RCM751>3.0.CO;2-J
- 795 38. Kaiser J, Brenninkmeijer CAM, Röckmann T. Intramolecular ¹⁵N and ¹⁸O fractionation in
796 the reaction of N₂O with O(¹D) and its implications for the stratospheric N₂O isotope
797 signature. *J Geophys Res Atmospheres.* 2002;107(D14):ACH 16-1-ACH 16-14.
798 doi:10.1029/2001JD001506
- 799 39. Kaiser J. *Stable Isotope Investigations of Atmospheric Nitrous Oxide.* Johannes Gutenberg
800 University of Mainz; 2003. <https://doi.org/10.25358/openscience-3976>
- 801 40. Röckmann T, Levin I. High-precision determination of the changing isotopic composition
802 of atmospheric N₂O from 1990 to 2002. *J Geophys Res Atmospheres.* 2005;110(D21).
803 doi:10.1029/2005JD006066
- 804 41. Yung YL, Miller CE. Isotopic Fractionation of Stratospheric Nitrous Oxide. *Science.*
805 1997;278(5344):1778-1780. doi:10.1126/science.278.5344.1778
- 806 42. Röckmann T, Kaiser J, Brenninkmeijer CAM, et al. Isotopic enrichment of nitrous oxide
807 (¹⁵N¹⁴NO, ¹⁴N¹⁵NO, ¹⁴N¹⁴N¹⁸O) in the stratosphere and in the laboratory. *J Geophys*
808 *Res Atmospheres.* 2001;106(D10):10403-10410. doi:10.1029/2000JD900822
- 809 43. Toyoda S, Yoshida N, Urabe T, et al. Temporal and latitudinal distributions of stratospheric
810 N₂O isotopomers. *J Geophys Res Atmospheres.* 2004;109(D8). doi:10.1029/2003JD004316
- 811 44. Kaiser J, Engel A, Borchers R, Rockmann T. Probing stratospheric transport and chemistry
812 with new balloon and aircraft observations of the meridional and vertical N₂O isotope
813 distribution. *Atmos Chem Phys.* Published online 2006:22.
- 814 45. Park S, Atlas EL, Boering KA. Measurements of N₂O isotopologues in the stratosphere:
815 Influence of transport on the apparent enrichment factors and the isotopologue fluxes to the
816 troposphere. *J Geophys Res Atmospheres.* 2004;109(D1). doi:10.1029/2003JD003731
- 817 46. Sutka RL, Ostrom NE, Ostrom PH, Gandhi H, Breznak JA. Nitrogen isotopomer site
818 preference of N₂O produced by *Nitrosomonas europaea* and *Methylococcus capsulatus*
819 Bath. *Rapid Commun Mass Spectrom RCM.* 2003;17(7):738-745. doi:10.1002/rcm.968
- 820 47. Sutka RL, Ostrom NE, Ostrom PH, et al. Distinguishing Nitrous Oxide Production from
821 Nitrification and Denitrification on the Basis of Isotopomer Abundances. *Appl Environ*
822 *Microbiol.* 2006;72(1):638-644. doi:10.1128/AEM.72.1.638-644.2006
- 823 48. Sutka RL, Ostrom NE, Ostrom PH, Gandhi H, Breznak JA. Nitrogen isotopomer site
824 preference of N₂O produced by *Nitrosomonas europaea* and *Methylococcus capsulatus*
825 Bath. *Rapid Commun Mass Spectrom.* 2004;18(12):1411-1412. doi:10.1002/rcm.1482

- 826 49. Toyoda S, Mutoh H, Yamagishi H, Yoshida N, Tanji Y. Fractionation of N₂O isotopomers
827 during production by denitrifier. *Soil Biol Biochem.* 2005;37(8):1535-1545.
828 doi:10.1016/j.soilbio.2005.01.009
- 829 50. Frame CH, Casciotti KL. Biogeochemical controls and isotopic signatures of nitrous oxide
830 production by a marine ammonia-oxidizing bacterium. *Biogeosciences.* 2010;7(9):2695-
831 2709. doi:10.5194/bg-7-2695-2010
- 832 51. Schmidt HL, Werner RA, Yoshida N, Well R. Is the isotopic composition of nitrous oxide
833 an indicator for its origin from nitrification or denitrification? A theoretical approach from
834 referred data and microbiological and enzyme kinetic aspects. *Rapid Commun Mass*
835 *Spectrom.* 2004;18(18):2036-2040. doi:10.1002/rcm.1586
- 836 52. Ostrom NE, Pitt A, Sutka R, et al. Isotopologue effects during N₂O reduction in soils and in
837 pure cultures of denitrifiers. *J Geophys Res Biogeosciences.* 2007;112(G2).
838 doi:10.1029/2006JG000287
- 839 53. Kaiser J, Park S, Boering KA, Brenninkmeijer CAM, Hilker A, Röckmann T. Mass
840 spectrometric method for the absolute calibration of the intramolecular nitrogen isotope
841 distribution in nitrous oxide. *Anal Bioanal Chem.* 2004;378(2):256-269.
842 doi:10.1007/s00216-003-2233-2
- 843 54. Westley MB, Popp BN, Rust TM. The calibration of the intramolecular nitrogen isotope
844 distribution in nitrous oxide measured by isotope ratio mass spectrometry. *Rapid Commun*
845 *Mass Spectrom.* 2007;21(3):391-405. doi:10.1002/rcm.2828
- 846 55. Ostrom NE, Gandhi H, Coplen TB, et al. Preliminary assessment of stable nitrogen and
847 oxygen isotopic composition of USGS51 and USGS52 nitrous oxide reference gases and
848 perspectives on calibration needs. *Rapid Commun Mass Spectrom.* 2018;32(15):1207-1214.
849 doi:10.1002/rcm.8157
- 850 56. Mohn J, Wolf B, Toyoda S, et al. Interlaboratory assessment of nitrous oxide isotopomer
851 analysis by isotope ratio mass spectrometry and laser spectroscopy: current status and
852 perspectives. *Rapid Commun Mass Spectrom.* 2014;28(18):1995-2007.
853 doi:10.1002/rcm.6982
- 854 57. Baertschi P. Absolute ¹⁸O content of standard mean ocean water. *Earth Planet Sci Lett.*
855 1976;31(3):341-344. doi:10.1016/0012-821X(76)90115-1
- 856 58. Jabeen I, Kusakabe M. Determination of δ ¹⁷O values of reference water samples VSMOW
857 and SLAP. *Chem Geol.* 1997;143:115-119. doi:10.1016/S0009-2541(97)00109-5
- 858 59. Kaiser J, Röckmann T, Brenninkmeijer CAM. Complete and accurate mass spectrometric
859 isotope analysis of tropospheric nitrous oxide. *J Geophys Res Atmospheres.*
860 2003;108(D15). doi:10.1029/2003JD003613

60. Kaiser J, Röckmann T. Correction of mass spectrometric isotope ratio measurements for isobaric isotopologues of O₂, CO, CO₂, N₂O and SO₂. *Rapid Commun Mass Spectrom.* 2008;22(24):3997-4008. doi:10.1002/rcm.3821
61. Kaiser J, Hastings MG, Houlton BZ, Röckmann T, Sigman DM. Triple Oxygen Isotope Analysis of Nitrate Using the Denitrifier Method and Thermal Decomposition of N₂O. *Anal Chem.* 2007;79(2):599-607. doi:10.1021/ac061022s
62. Wankel SD, Ziebis W, Buchwald C, et al. Evidence for fungal and chemodenitrification based N₂O flux from nitrogen impacted coastal sediments. *Nat Commun.* 2017;8(1):1-11. doi:10.1038/ncomms15595
63. Magyar PM, Orphan VJ, Eiler JM. Measurement of rare isotopologues of nitrous oxide by high-resolution multi-collector mass spectrometry. *Rapid Commun Mass Spectrom.* 2016;30(17):1923-1940. doi:10.1002/rcm.7671
64. Kelly CL. ckelly314/pyisotopomer: v1.0.4. Published online January 19, 2023. doi:10.5281/zenodo.7552724
65. McIlvin MR, Casciotti KL. Technical updates to the bacterial method for nitrate isotopic analyses. *Anal Chem.* 2011;83(5):1850-1856. doi:10.1021/ac1028984
66. McIlvin MR, Casciotti KL. Fully automated system for stable isotopic analyses of dissolved nitrous oxide at natural abundance levels. *Limnol Oceanogr Methods.* 2010;8(2):54-66. doi:10.4319/lom.2010.8.54
67. Scott KM, Lu X, Cavanaugh CM, Liu JS. Optimal methods for estimating kinetic isotope effects from different forms of the Rayleigh distillation equation 1 Associate editor: J. Horita. *Geochim Cosmochim Acta.* 2004;68(3):433-442. doi:10.1016/S0016-7037(03)00459-9
68. LI W. Measurement of the absolute abundance of oxygen-17 in V-SMOW. *Chin Sci Bull.* 1988;33:1610-1613. Accessed June 10, 2021. <https://ci.nii.ac.jp/naid/80004607415/>
69. Santoro AE, Buchwald C, McIlvin MR, Casciotti KL. Isotopic Signature of N₂O Produced by Marine Ammonia-Oxidizing Archaea. *Science.* 2011;333(6047):1282-1285. doi:10.1126/science.1208239
70. Dutton GS, Elkins JW, Hall BD. Nitrous Oxide data from the NOAA/ESRL halocarbons in situ program. Published online 2021. Accessed November 19, 2021. <https://data.nodc.noaa.gov/cgi-bin/iso?id=gov.noaa.ncdc:C01556>
71. Röckmann T, Kaiser J, Brenninkmeijer CAM, Brand WA. Gas chromatography/isotope-ratio mass spectrometry method for high-precision position-dependent ¹⁵N and ¹⁸O measurements of atmospheric nitrous oxide. *Rapid Commun Mass Spectrom.* 2003;17(16):1897-1908. doi:10.1002/rcm.1132

- 896 72. Glover DM, Jenkins WJ, Doney SC. *Modeling Methods for Marine Science*. Cambridge
897 University Press; 2011. doi:10.1017/CBO9780511975721
- 898 73. Lorquet JC, Cadet C. Excited states of gaseous ions: I. Selection rules in photoelectron
899 spectroscopy and photoionization. The case of N₂O⁺. *Int J Mass Spectrom Ion Phys*.
900 1971;7(3):245-254. doi:10.1016/0020-7381(71)80020-7
- 901 74. Märk E, Märk TD, Kim YB, Stephan K. Absolute electron impact ionization cross section
902 from threshold up to 180 eV for N₂O+e→N₂O⁺⁺+2e and the metastable and collision
903 induced dissociation of N₂O⁺. *J Chem Phys*. 1981;75(9):4446-4453. doi:10.1063/1.442611
- 904 75. Bigeleisen J. Chemistry of Isotopes. *Science*. 1965;147(3657):463-471.
905 doi:10.1126/science.147.3657.463
- 906 76. Begun GM, Landau L. Metastable Transitions in N₂O⁺. *J Chem Phys*. 1962;36(4):1083-
907 1084. doi:10.1063/1.1732641
- 908
909

Table 1. Reference materials for N₂O isotopic analysis and intercalibration. Except for one internal standard (B6), calibrated values were provided via independent measurement by S. Toyoda, Tokyo Tech., J. Mohn, EMPA; or, in the case of tropospheric N₂O, the 2018 annual average measured at Jungfraujoch, Switzerland, reported by Yu et al. (2020). The laboratories participating in the intercalibration exercise were at Stanford University (“Lab 1”) and the University of Basel (“Lab 2”). ³¹R values represent the inherent, unscrambled ³¹R of each reference material, calculated from eqn. (6).

Reference material	Matrix	Mole fraction μmol mol ⁻¹	δ(¹⁵ N ^α)	δ(¹⁵ N ^β)	δ(¹⁵ N ^{sp})	δ(¹⁵ N ^{bulk})	δ(¹⁸ O)	³¹ R (¹⁵ R ^{α+17} R)	⁴⁵ R	⁴⁶ R	Calibration by
			(‰, vs. air N ₂)				(‰, vs. VSMOW)				
S2 reference gas	Synthetic air	90	5.55	-12.87	18.42	-3.66	32.73	0.004083	0.007712	0.002087	Toyoda & Mohn
B6 reference gas	He	900	-0.40	-0.15	-0.26	-0.28	41.95	0.004063	0.007739	0.002106	Lab 1 internal standard
Tropospheric N ₂ O (2018 annual average)	Air	~0.33	15.6	-2.3	17.9	6.6	44.4	0.004123	0.007787	0.002111	Yu et al. (2020)
CA06261	Synthetic air	90	-22.21	-49.28	27.07	-35.75	26.94	0.003980	0.007475	0.002075	Toyoda & Mohn
53504	Synthetic air	90	1.71	94.44	-92.73	48.08	36.01	0.004070	0.008093	0.002095	Toyoda & Mohn
CA08214	Synthetic air	90	17.11	-3.43	20.54	6.84	35.39	0.004126	0.007790	0.002093	Toyoda & Mohn
90454	Synthetic air	90	25.73	25.44	0.29	25.59	35.88	0.004158	0.007928	0.002094	Toyoda & Mohn
94321	Synthetic air	90	50.52	2.21	48.31	26.37	35.54	0.004249	0.007934	0.002094	Toyoda & Mohn
Lab 1 pure N ₂ O direct injection ("A01")	Pure N ₂ O	N/A	0.24	0.12	0.13	0.18	39.85	0.003734	0.007742	0.002101	Toyoda
Lab 2 pure N ₂ O direct injection	Pure N ₂ O	N/A	-4.07	3.59	-7.66	-0.24	39.25	0.004044	0.007739	0.002100	Mohn

Table 2. N₂O isotopic composition of reference materials and two unknowns analyzed by two IRMS laboratories, calculated using γ and κ values determined from reference materials 53504 and CA08214 with the algebraic solution. $\delta(^{15}\text{N}^\alpha)$, $\delta(^{15}\text{N}^\beta)$, $\delta(^{15}\text{N}^{\text{sp}})$ and $\delta(^{15}\text{N}^{\text{bulk}})$ are reported in ‰ vs. Air N₂, and $\delta^{18}\text{O}$ is reported in ‰ vs. VSMOW. Uncertainties are standard deviations of replicate bottles and do not include calibration uncertainties. The root-mean square deviation (RMSD) was calculated with respect to calibrated values.

Reference material		<i>n</i>	$\delta(^{15}\text{N}^\alpha)$	σ	$\delta(^{15}\text{N}^\beta)$	σ	$\delta(^{15}\text{N}^{\text{sp}})$	σ	$\delta(^{15}\text{N}^{\text{bulk}})$	σ	$\delta(^{18}\text{O})$	σ
			(‰, vs. air N2)						(‰, vs. VSMOW)			
CA06261	Calibrated value		-22.2		-49.3		27.1		-35.7		26.9	
	Lab 1	4	-20.6	1.3	-50.5	1.3	29.9	2.7	-35.6	0.2	28.4	0.8
	Lab 2	16	-20.5	1.4	-50.9	2.6	30.4	3.8	-35.7	1.0	27.6	1.8
	RMSD		2.3		2.1		4.4		0.2		1.5	
53504	Calibrated value		1.7		94.4		-92.7		48.1		36.0	
	Lab 1	4	0.0	1.0	95.7	2.1	-95.7	2.5	47.9	1.1	37.6	0.8
	Lab 2	15	1.7	1.0	94.5	1.9	-92.8	2.9	48.1	0.6	36.4	1.6
	RMSD		1.7		1.3		3.0		0.2		1.7	
CA08214	Calibrated value		17.1		-3.4		20.5		6.8		35.3	
	Lab 1	6	17.0	2.0	-2.4	0.9	19.4	2.9	7.3	0.7	36.3	1.4
	Lab 2	16	17.0	1.1	-3.2	0.7	20.2	1.3	6.9	0.6	36.0	3.6
	RMSD		0.1		1.1		1.2		0.5		1.3	
Tropospheric N ₂ O	Calibrated value		15.6		-2.3		17.9		6.6		44.4	
	Lab 1	7	15.1	0.8	-2.5	2.3	17.5	2.8	6.3	1.0	43.1	2.1
	Lab 2	2	15.8	1.1	-3.7	0.0	19.5	1.0	6.1	0.5	44.7	1.0
	RMSD		0.6		1.4		1.7		0.6		1.3	
B6	Calibrated value		-0.4		-0.1		-0.3		-0.3		41.9	
	Lab 1	7	-2.2	0.7	1.3	1.0	-3.4	1.2	-0.4	0.7	41.5	1.6
	RMSD		1.8		1.4		3.2		0.2		0.5	
S2	Calibrated value		5.6		-12.9		18.4		-3.7		32.7	
	Lab1	6	5.0	0.5	-13.1	1.6	18.1	1.3	-4.0	1.0	31.5	1.8
	RMSD		0.5		0.2		0.3		0.4		1.2	
Lake Lugano, 10m	Lab 1	3	13.2	0.3	-5.6	1.2	18.8	1.5	3.8	0.4	44.6	1.2
	Lab 2	5	14.8	1.5	-6.6	1.3	21.4	2.5	4.1	0.5	45.5	0.6
Lake Lugano, 90m	Lab 1	3	19.2	0.5	-33.1	0.7	52.3	1.2	-6.9	0.1	56.8	0.1
	Lab 2	2	18.5	0.8	-32.4	0.3	50.9	0.5	-6.9	0.5	55.4	1.9

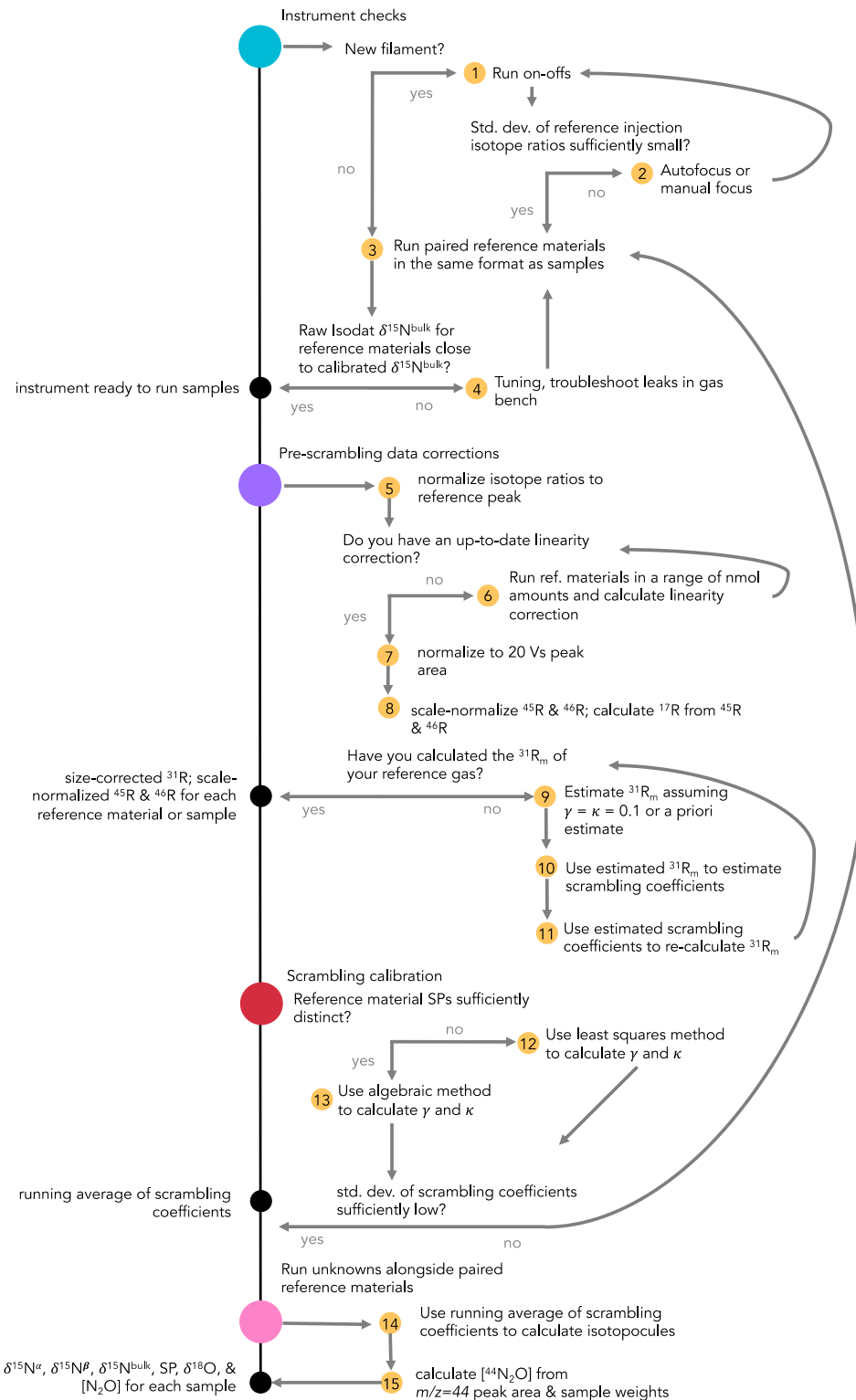


Figure 1. N₂O data corrections flowchart. Instrument checks, pre-scrambling data corrections, the scrambling calibration, and isotopomer calculations are laid out; numbers in yellow circles correspond to step numbers referred to in the text. Steps 1-4 are performed with raw Isodat output, steps 5-8 are accomplished in the data corrections spreadsheet template, step 9 is a simple calculation, and steps 10-14 are accomplished with the pyisotopomer code.

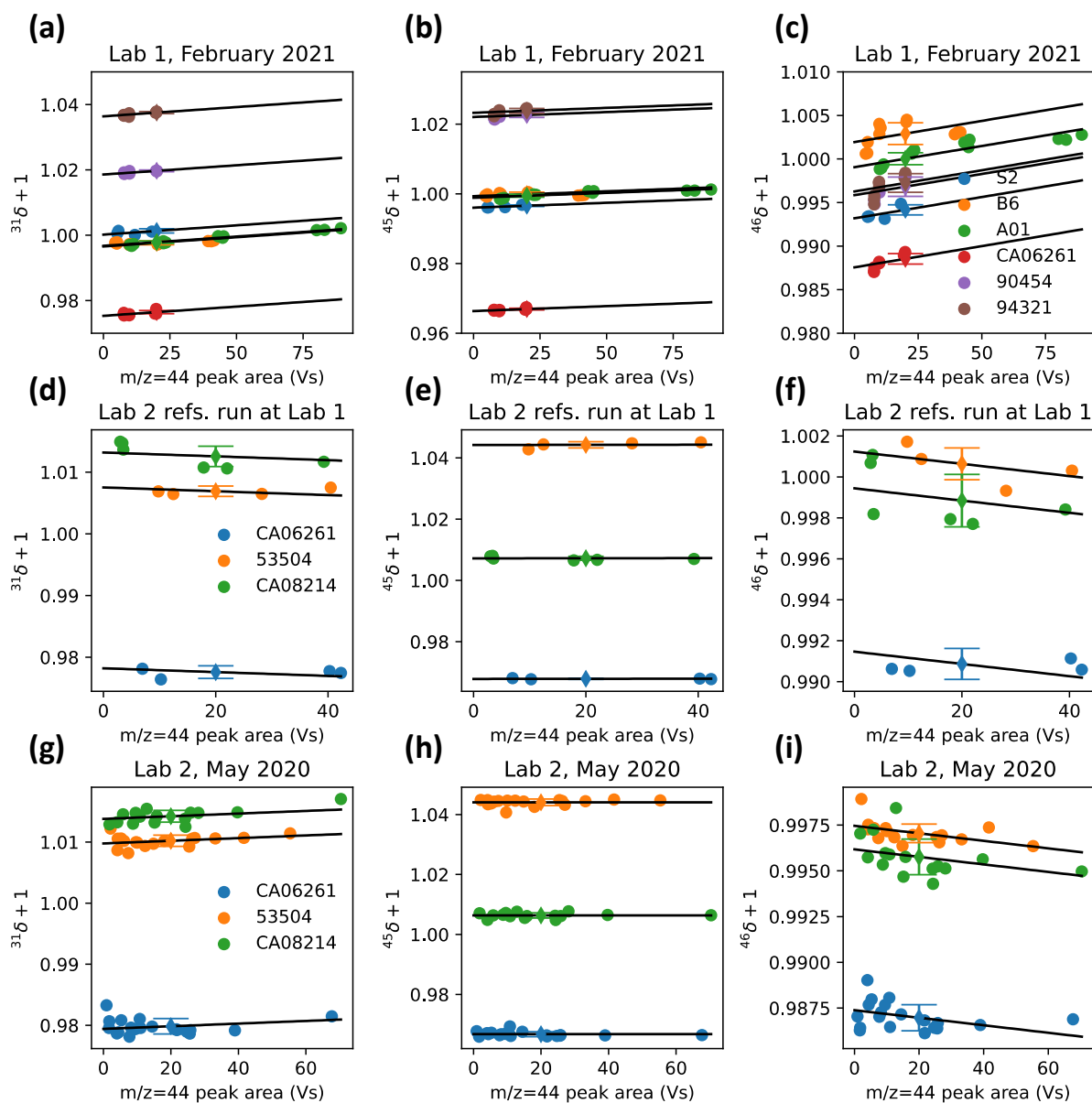


Figure 2. Linearity relations for reference materials used to normalize measured isotope ratios to a peak area of 20 Vs, using the dummy variable method⁶⁷. $^{31}\delta+1$ (a,d,g), $^{45}\delta+1$ (b,e,h), and $^{46}\delta+1$ (c, f, i) are plotted against m/z 44 peak area. Linearity relations are shown for reference materials prepared and run in Lab 1 (a-c), reference materials prepared in Lab 2 but run in Lab 1 (d-f), and reference materials run in Lab 2 (g-i). A common slope (black line) calculated from the dummy variable method for each molecular ion ratio is overlain on each data series (colored circles). The estimated isotope ratio corresponding to a peak area of 20 Vs is also shown for each series (colored diamonds, error bars correspond to the standard error of the predicted y-value).

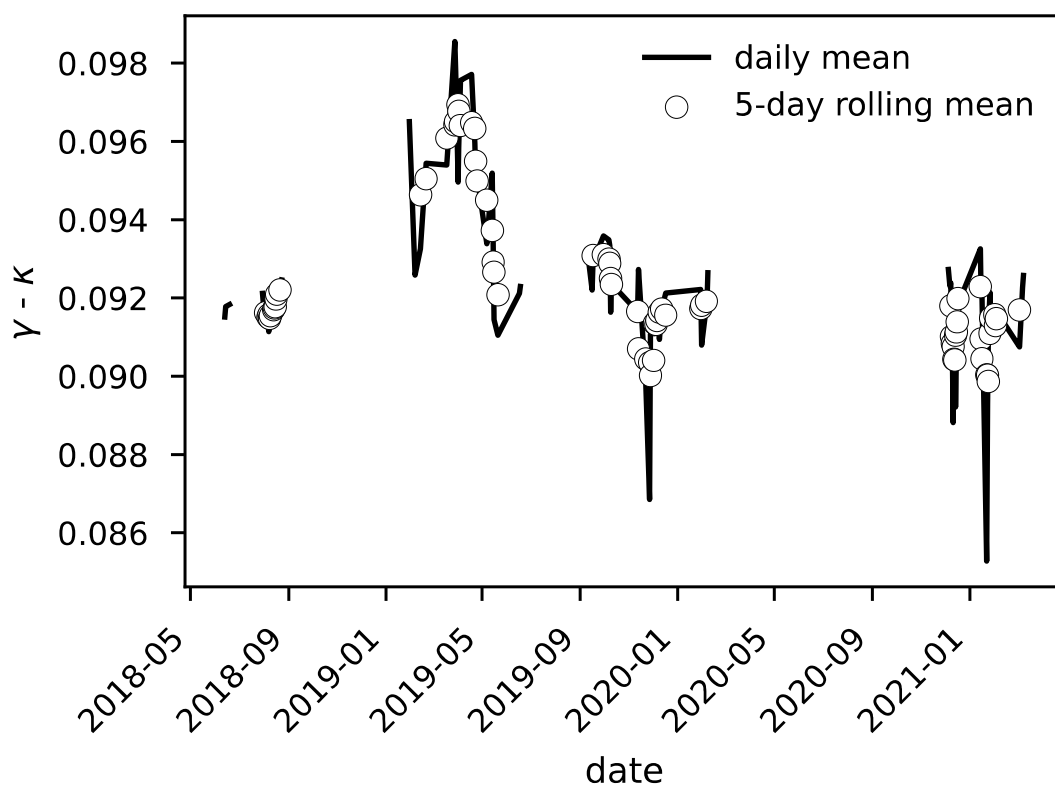


Figure 3. $\gamma - \kappa$ for the Lab 1 IRMS from June 2018 to March 2021. Daily mean $\gamma - \kappa$ (black line) values are plotted with a 5-day rolling average (dots).

